p-32

CR-189435

Final Report for NASA PO S-97229-E (CSC Task #5797), Voyager GO Program

Myron Smith, CSC/Science Programs

This contract pertained to the investigation of the time variability of the ultraviolet continuum flux of three stars, lambda Eri, 53 Persei, and and gamma Cas. The observations were conducted in 1991 and were provided to the Principal Iinvestigator in December of 1992. The investigator traveled to Tucson, Arizona to reduce the data in February of 1993 and analyzed the data during the spring and summer of 1993.

The Voyager observations of 53 Persei were conducted simultaneously with a global ground-based campaign of visual-wavelength photometry. The optical campaign established beyond doubt the existence of two nonradial pulsation modes with periods near two days. Using the ephemeris from the ground-based campaign we were able predict the time variability for the optical results with one unknown parameter. The Voyager results showed the variability with the predicted period and phase, permitting us to determine the amplitude in the ultraviolet. Combining the visual and ultraviolet amplitudes, we were able to compare their ratio with that predicted for nonradial pulsation modes from theory. Our results show that the pulsation modes of this star can be described by a spherical harmonic index, l, of 2 or 1 (less probable). A scientific paper summarizing these results was published in the Proceedings of the IAU Colloq. 162 in 1994.

The second part of the program concerned the ultraviolet continuum modulations of the B2e star lambda Eri. These observations were conducted in November, 1990. The data were combined with IUE and optical data and published in a paper cited below as Smith and Polidan 1993 and Smith 1994b.

Voyager observations of lambda Eri showed that the ultraviolet light curve of lambda Eri shows no variations over a timescale of a day, but may show excursions on the order of an hour. There was little actual overlap between the Voyager and IUE datasets in time so we could not determine whether the short-term variations from Voyager are instrumental or from the star. However, the absence of variations at times coinciding with the formation of spectral transients called "dimples" in the optical lines of this star puts important upper limits on the masses of the plasma structures responsible for the dimples.

The third and final part of the program concerned the ultraviolet continuum variations of the B0.5 star gamma Cas. These data were obtained in 1990 and 1991. The results were submitted to the Astrophysical Journal and are scheduled to be published in their April 1, 1995 issue (see below).

The Voyager observations of gamma Cas show that 10-20% variations occur on a timescale of 1-2 hrs. and are commonplace. A difference spectrum formed from high and low flux states shows a spectrum indistinguishable from the low-state (photospheric) spectrum. Moreover, a histogram formed from the differences of flux from adjacent observations is very similar to histograms formed from light curves from two x-ray satellites, suggesting that the ultraviolet and x-ray continuum variations have the same origin. If correct, this association casts doubt on the popular view that the x-ray emission from this star arises from a wind-fed accretion disk around a degenerate companion to this star. Rather, we suggest that the x-ray emission arises from localities near the surface of the Be star itself.

Photospheric Activity in Selected Be Stars: λ Eri and γ Cas

Myron A. Smith,
IUE/CSC Observatory, 10000A Aerospace Rd., Lanham-Seabrook MD 20706, USA

Abstract. Recent observations of rapid variations in optical He I lines, X-rays, and FUV wavelengths in the prototypical classical Be stars λ Eri and star γ Cas hint that the violent processes occur on the surfaces of these stars most all the time. We suggest that of these phenomena show greater similarities with magnetic flaring than any other process thought to occur on stars.

1 Introduction

In retrospect, Peters's (1986) observation of the development of a high velocity feature in the λ6678 profile of μ Cen (B2e) was a call for the Be community to recognize that mass ejections of the surfaces of Be stars can occur discretely and violently over very rapid timescales. The extension of monitoring observations over several wavelength regimes, together with the development of multi-line spectroscopic detectors has brought necessary new tools to the search for the instability mechanism(s) in the atmospheres of classical Be stars. A reasonable strategy for investigating the local sites of mass ejections is to focus on a mild Be star the surface of which is visible most of the time because the outburst duty cycle is low, and a very active Be star seen at intermediate inclination. Examples of each of these categories are λ Eri (near edge-on, B2e; outburst duty cycle $\sim$20%) and γ Cas (B0.5e; in emission for 50 years), and I will confine my discussion to them. In addition to work by our group at Goddard, other teams have initiated *rapid* spectroscopic variability programs on these stars, e.g. in the U.S. (Gies, Peters), Canada (Kambe, Walker), Japan (Hirata), and India (Anandarao, Ghosh).

2 λ Eri's He I Line "Dimples"

In addition to regular line profile variations (*lpvs*) generally attributed to NRP, the He I λ6678 line of λ Eri shows an almost constant erratic activity which can be fit into a small group of patterns known as spectral transients (e.g. Smith 1989). At least 60% of these events appear as central absorptions and weak flanking emissions known as "dimples" along the λ6678 profile. An additional $\sim$10% are "type d" or pure absorption events which are probably related to dimples. These features have a frequency of 1.3 ± 0.3 events nt^{-1} and a duration of 2-4 hrs. They show a slow drift to the red during their lifetime. Occasionally, dimples have been observe to "come and go" over several hours, all the while moving along the profile consistent with the stellar rotation rate, as if caused by a rooted active spot on the surface. With the exception of two possible simultaneous dimples in the λ4922, dimples have been observed only in λ6678. Smith and Polidan (1993; SP) note that the λ6678 line in five other Be/Bn stars with Vsin i $\geq$ 250 km s^{-1} show dimples.

In a simultaneous optical/*IUE* campaign, SP discovered that 10-20% weakenings of the C IV and N V resonance doublets were correlated with the appearance of λ6678 dimples. This discovery suggested plasma had been added along the line-of-sight with a density in between those in which the C IV and λ6678 lines normally form. This indication, along with the observation that the λ6678 line conserves its EW during a dimple appearance, led SP to investigate an *ad hoc* model for a dimple consisting of an opaque (in λ6678) stationary, detached, intermediate density "slab" over the surface of λ Eri that backscatters line photons back toward the star. Photons scattered a second time in a "penumbra" surrounding the slab's projection on the surface acquire a doppler shift from the local projected rotational velocity, thereby redistributing photons from the central absorption part of the feature into wings with slightly enhanced emission. The model predicts the slabs' areas, elevations over the star, vertical velocity, and also permits estimates of slab densities. Typical slabs show areas of $\sim$3% of the star's area, an elevation of $0.1R_*$, and a density of 10^{11-12} cm^{-3}. A slab cannot be associated with material moving with a vertical velocity exceeding the line width, for otherwise the slab will become transparent to λ6678 flux and the dimple will disappear. Typically, $V_{vert} \leq 30$ km s^{-1}. SP show that even some bizarre-shaped dimples with "inverse-P Cygni" profiles can be modeled with a slab falling at $\sim$35 km s^{-1} and also having an azimuthal component. If one assumes that 1.5 slabs are present somewhere over λ Eri's surface at any one time, they must comprise $\geq 3\times10^{-14}$ $M_\odot$. If dimples are visible in λ4922 the lower limit becomes 2×10^{-13} $M_\odot$. Given these masses, slabs should be just detectable over λ Eri as Hα emission (Marlborough 1993).

Dimples become optically thick within 15 mins. of onset (SP). This fact and the derived area means that the disturbance responsible for them propagates at $\sim$800 km s^{-1}, or about V_{esc}. One may discount formation scenarios requiring dimple-slabs to arise either from stellar ballistic ejections (dimples last too long) or from orbiting circumstellar debris (not long enough). Perhaps an Alfvenic disturbance propagates at this velocity, but this would not explain how plasma material can be transported at many times the sound speed to form a condensation. A paradigm that does account for many of the properties of slabs is the impulsive solar flare, which ejects a high energy plasma/electron beam to the chromo-/photosphere and heats it to a high temperature. The heated material evaporates from the surface at a velocity close to V_{esc} and encounters coronal magnetic loops, causing it to pile up there. The evaporate cools to become a visible condensed prominence and eventually slowly falls back to the surface along field lines The decay timescale for prominences is slow, $\sim$2 days, compared to dimple lifetimes, but the formation timescale, density, and elevation over the Sun are similar to SP's estimates from modeling λ Eri's dimples.

Although the doppler integration models of dimples fit their shapes, we are unable to reproduce intensity line profiles from NLTE models with black line-cores, as implicitly required by SP's backscattering model. This failure exemplifies the present lack of understanding of the physics of formation of these He I lines.

3 Multi Line Observations of Rapid Emission Activity in λ Eri

One way to study the line formation process is to compare and model the simultaneous response of several lines arising from the same atom. Toward this end we obtained (Smith et al. 1994) three nights of time series of KPNO fiber-echelle spectra of the first two members of the He I singlet/triplet 2P – nD series, *viz.* λ6678, λ4922, λ5876, and λ4471 when λ Eri happened to be in emission. Time serial observations of λ Eri, μ Cen, γ Cas and other stars in their active phases has demonstrated that emission features in He I lines (and sometimes even Hα) can show substantial variability in much less than the star's rotation period. λ Eri's λ6678 rapid emission variablity often falls into one of several patterns that suggests the occurrence of failed ejections (see e.g. Smith 1989). This includes high velocity blue absorption components, emission shifting continuously from the V to the R wing on a timescale consistent with the ejection/infall velocities, and a correlation of blue absorptions followed shortly by red emissions. R emissions can even evolve into higher velocity absorptions as infalling material crosses the line of sight to the stellar disk (Smith et al. 1991; "SPG91"). Thin rings of material orbiting within 1R$_*$ of the surface have also been noted (SPG91). It should therefore not be surprising that much of the V/R emission comes from matter projected over the limb matter. However, in general it is difficult to distinguish between emission produced by over-the-limb material and foreground matter with an enhanced source function. In the case of λ Eri, the potential exists for this ambiguity to be broken because R emissions tend to be stronger and because they are more prevalent than V emissions (Smith 1989).

The means to break the geometrical ambiguity was provided by simultaneous observations of several He I lines using Kitt Peak's 2.1-m echelle spectrograph on 1991 November 3-5 (Smith et al. 1994). We monitored the first two members of the singlet and triplet 2P – nD series, *viz.* λ6678, λ4922, λ5876, and λ4471. Our data showed contrasting behaviors of the V, R emission in the line wings and inner profile in this way: V emissions tend to scale with the line's log gf, with the blue lines showing small or no emission as the red lines varied from large to moderate emission strengths. Increases in R-wing emission correlated with definite weak *absorptions* in the V-wing of λ4922. When the "excess" emission wanes in λ6678 so does the absorption in λ4922. Figures 1 shows an example of this contrasting behavior. Figure 2 shows emission/absorption in the red cores of the two lines.

This behavior must necessarily be interpreted through NLTE processes affecting atoms in *foreground* material. Using the sophisticated NLTE code TLUSTY written by Hubeny (1988), Smith et al. (1994) were able to understand the simultaneous emission and absorption of these two lines by an NLTE effect first noted by Auer and Mihalas (1972) in hot atmospheres ($T_{eff} \geq 45000$K). At these temperatures, He I becomes a trace ion, causing the λ584 resonance line to become transparent and its radiation to leave the star. This drains electrons from the lower state of λ6678, 2^1P, thereby enhancing the source function of all transitions

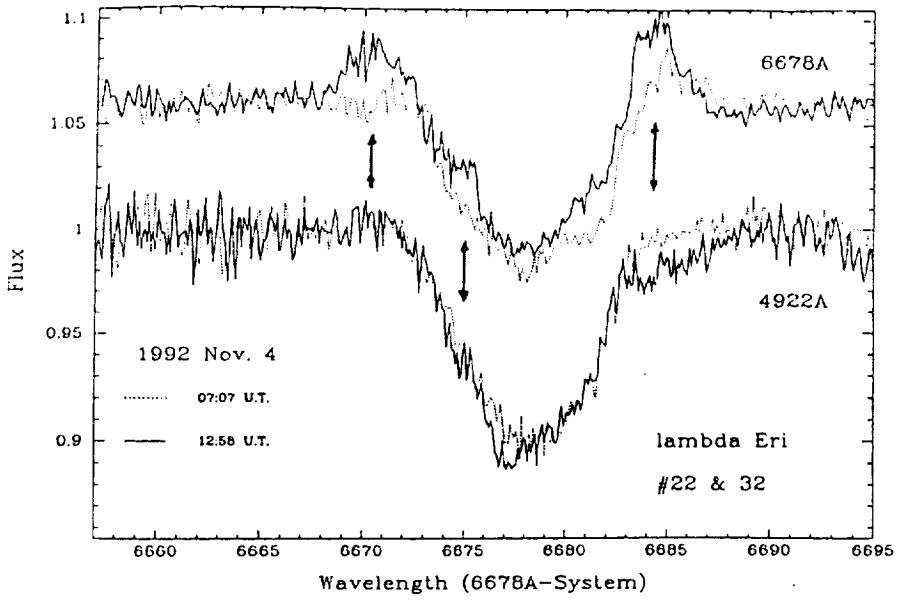

Fig. 1 – λ Eri's R-wing fluctuations in emission (λ6678) and absorption (λ4922). Note V-wing/core emission in λ6678 compared to no change in λ4922.

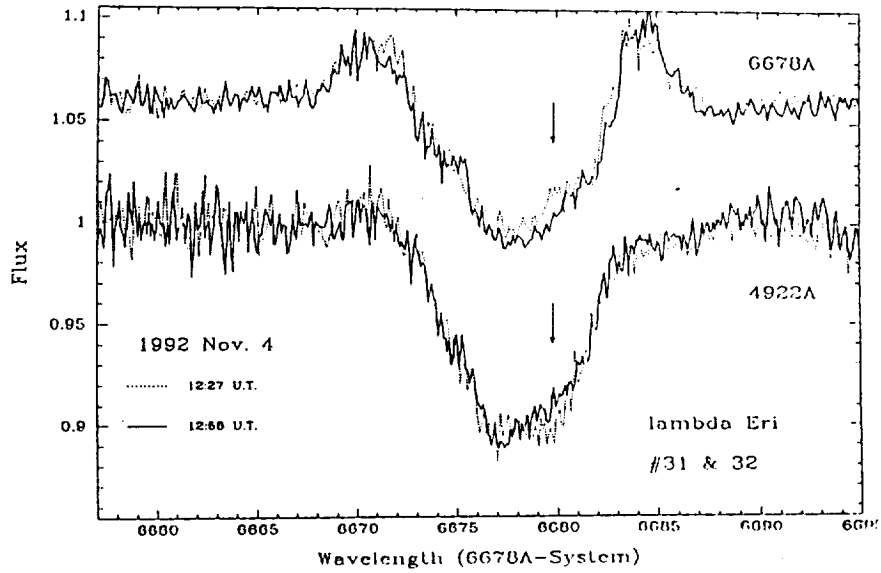

Fig. 2 – Simultaneous em., abs. fluctuations in the red core of λ6678, λ4922.

from this level. The effect is augmented for λ6678 by stimulated emission, driving the line almost preferentially into emission. Further study shows that this mechanism is confined to plasmas with at least a photospheric density. This is because at lower densities corresponding to the same ionization state the temperature and UV radiation field are too low to populate the upper atomic levels substantially, and this decreases the source function of all these lines. As *Figure 3* shows, the combination of λ6678 excess emission and λ4922 absorption confines the region of the (T_{eff}, log g) (i.e. T, N_e) domain further, requiring temperatures of at least 40000 K and densities of $\geq 10^{14}$ cm^{-3}. Another implication of this diagram is that the region where the required emission/absorption occurs does not coincide with the requirements for greatest efficiency of λ6678 emission. This implies that a much larger area of the star is responsible for λ6678 emission than if there were no λ4922 absorption. We plan to estimate typical hot spot areas in the near future.

The TLUSTY results imply that in contrast to the V-wing, the emission from the R-wing during λ Eri's outburst phase probably arise from downward-moving plasma within the atmosphere itself. It is easy to show from Virial Theorem arguments that the liberation of gravitational potential energy by infalling matter is too weak by $\geq 10^{4-5}\times$ to heat the implied hot spots on the star down to a level $\tau_c \sim 10^{-3}$. In contrast, there is enough CS mass around Herbig Be stars like HR 5999 to power the emission of lines by an infall mechanism (Blondel et al. 1993). In the energy hierarchy of astrophysical energy mechanisms, gravity is rather powerful.

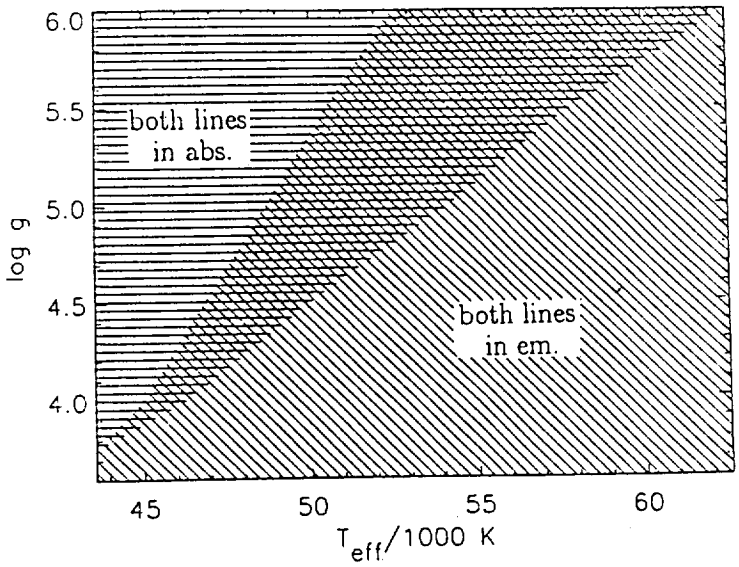

Fig. 3 – T_{eff}, log g diagram, showing range of λ6678 emission, λ4922 absorption (cross-thatched region).

It dwarfs almost all other energy sources operating on stellar surfaces. We are able to think of only one other source (excepting nucleosynthesis), *viz.* flaring, that can produce more energy. Once again magnetic energy dissipation seems implicated as a destabilizing mechanism in the atmosphere of λ Eri.

4 An X-Ray Flare on λ Eri

All this talk about possible flaring on λ Eri led us to request and be granted 29 Ksec of pointed (PSPC) observations with *Rosat*, an instrument capable of photon counting and spectral binning in the range 0.2-2 keV. Our observations were conducted on 1991 February 21-22 at the very beginning of the AO1/GO period with little notice to arrange simultaneous observations at other wavelengths. However, we were able to obtain an SWP camera *IUE* spectrum within several hours of the completion of the X-ray observations.

As detailed in Smith et al. (1993), our observations were distributed over 13 orbits spanning 38 hours. During the first two and last six orbits λ Eri was detected and showed a L_x/L_{bol} $\sim 2\times10^{-7}$ typical for an early B star. During the middle five orbits the X-ray flux rose to seven times its initial value; the e-folding timescale was $\leq$2 orbits. After reaching a peak $L_x = 4\times10^{31}$ ergs s^{-1}, the emission began declining, though with a slower decay rate. No significant fluctuations in emission were found on a shorter timescale. The final orbits of our timeline coincide with one rotational cycle after the maximum. Since the flux had returned to its initial state, one can rule out a rotationally modulated hot spot and characterize the brightening as an extended ($\sim$50,000 sec) flare, and a giant flare at that. The spectral analysis of our data shows the flare energy comes exclusively from photons having energies $\geq$ 0.7 keV and is characterized by a Raymond-Smith temperature of 1.4×10^7K and an Emission Measure of 3×10^{53} cm^{-3}. Both the temperature and EM of the softer component, presumably arising from the basal flux entirely, are each seven times smaller than the flare values.

The *IUE* spectrum showed a typically low wind flux for λ Eri, so that even if there was a hypothetical neutron star or white dwarf orbiting around this star too little X-ray flux would be emitted to account for the flare. As well as showing no detectable radial velocity variations that would betray binary motion, λ Eri's spectrum does *not* show traces of strong metal lines expected from a G-K dwarf capable of producing RS CVn-like or T Tauri flares. Smith et al. (1994) concluded that the best hypothesis was that this X-ray activity came from the Be star itself and probably from a flare-related process.

λ Eri is the second star to have been reported as an X-ray Be star; the first is γ Cas. The latter is well known to undergo rapid, chaotic X-ray fluctuations with a Raymond-Smith temperature of $\sim1.5\times10^8$K (Horaguchi et al. 1993, Parmar et al. 1993), if a thermal description is appropriate. Peters (1982) noted the first X-ray flare, an event on 1977 January 28 that was recorded as emission in several UV metallic lines as well as Hα (Slettebak and Snow 1978). Murakami et

al. (1986) recorded a flare spectrum lasting several minutes and a having a high temperature. Coincidentally or not, Yang et al. (1988) noted λ6678 line profile transients in observations a few days before this flare. Whereas the prevailing sentiment among the X-ray community is that γ Cas is a member of the group of X-ray Be binaries, the evidence for binarity is weak (no detectable RV variations; also, it has a symmetrical disk resolved by optical interferometry (e.g. Quirrenbach, these proc.). Thus it does not fit into that group easily. Perhaps the best argument that γ Cas has a close degenerate companion is the high temperature of its X-ray spectrum. In most other respects the argument for flares arising the Be star, in our opinion, equal or outweigh the mass-accretion/neutron star scenario.

It is difficult to prove that γ Cas and λ Eri are typical Be stars. Why, for example, do surveys show early Be stars to be normal, even subnormal X-ray emitters, (Berghofer and Schmitt, these proc.), when these two stars are so active? A possible explanation is that the X-ray emission occurs very close to the star and is attenuated by well developed Be disks. If so, the two stars we are discussing could be coincidentally good X-ray monitoring candidates either because the star's surface is usually visible or because X-ray flux is not absorbed by disks owing to a low aspect to our line of sight. We suggest that other low-sin i Be stars, e.g. μ Cen, should be good candidates for X-ray monitoring.

5 Far-UV and X-ray Activity Correlations in γ Cas

Our suspicion that the X-ray variability in γ Cas is produced near the Be star motivated us to request *Voyager 1* observations. Our request was granted, and we have obtained 1990-91 UVS data using the reduction program of Holberg and Watkins (1992) for calibration and descattering. The result is a series of 9.3Å-resolution spectra over the range $\lambda\lambda$930-1650 (except for poor sensitivity in $\lambda\lambda$1200-1360). We grouped our data into 61 useable 0.5-1 hr. bins of spectra. A temporal plot of monochromatic FUV fluxes (subset shown in Figure 4) shows that variability over the shortest timescales we could compare binned spectra to, 0.5–2 hrs., dominates any possible longer timescale variations. These variations can exceed 0.2 mags.

To understand the nature of these rapid fluctuations we performed two analyses. First, we used all the spectra to synthesize the spectrum of the fluctuating FUV component. This was constructed at each wavelength by subtracting the flux of the third brightest spectrum from the third faintest. The result, shown in Figure 5, is an almost white difference spectrum, except for a marginal enhancement at the Lyβ and Lyγ lines. Because this component has the same spectrum, the origin of the FUV variations is likely to be close to or even in the photosphere, not a hot site somewhere else. Second, we constructed a histogram of monochromatic flux differences (absolute value) between consecutive time binned observations $\sim$1 hr. apart. This is shown in Figure 6a. Note the flat-topped distribution out to a limit of 0.2 mags., beyond which there are few observations. This suggests that the fluctuating FUV component comes from several independent sources at any time.

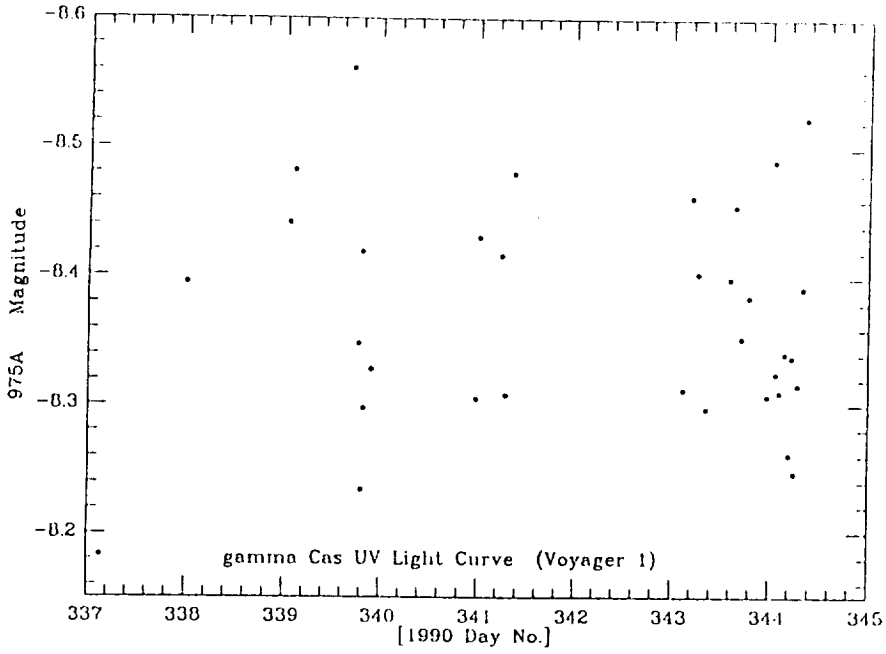

Fig. 4 – FUV rapid flux variations in γ Cas during 1990-1.

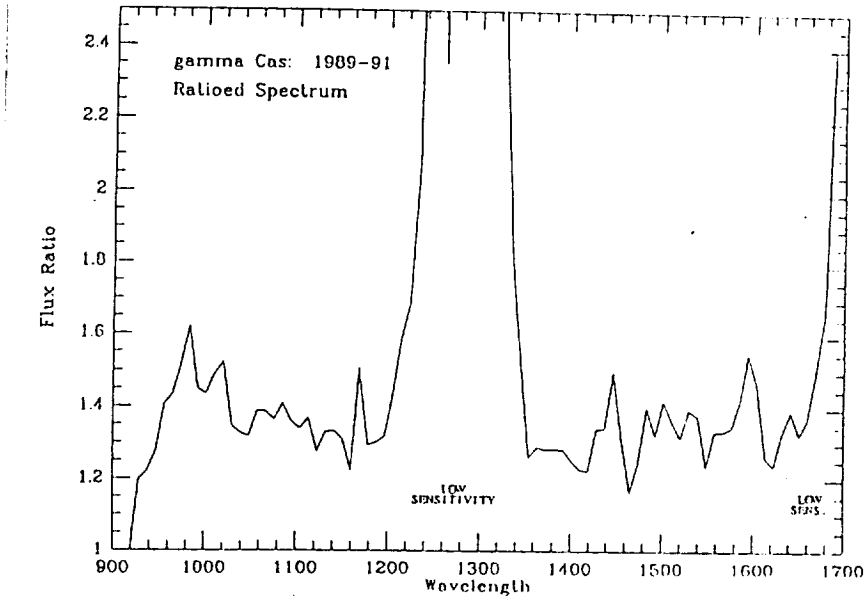

Fig. 5 – Derived spectrum of FUV fluctuating component of γ Cas.

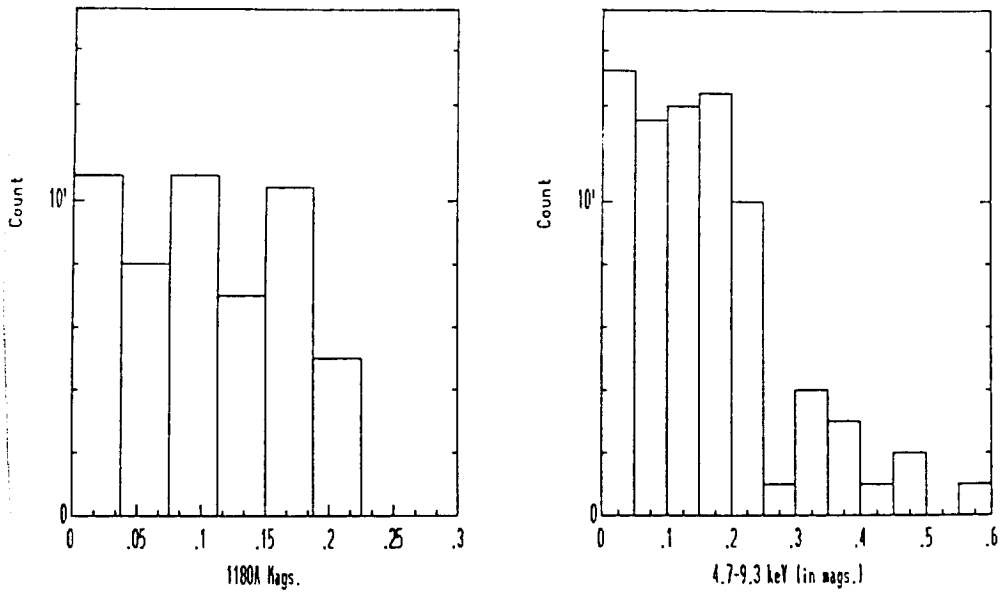

Fig. 6 – Histogram comparison of rapid FUV and X-ray flux variations of γ Cas.

To compare the FUV with the X-ray variations, we performed the same histogram analysis on the mean fluxes of consecutive orbits from the Parmar et al. (1993; *Exosat*; 5-9 keV) dataset in Figure 6b and the Horaguchi et al. (1993; *Ginga*; 1-9 keV) data (not shown). The FUV and X-ray distributions are nearly identical in shape and magnitude threshold. Further investigation shows that the histogram form holds for data grouped even 0.5 hr apart. In view of these similarities, we suggest that the FUV and X-ray variabilities have the same origin.

What could this origin be? The energy of the fluctuating X-rays is too high for them to arise from gravitational potential energy on the surface of the Be star. The energy in the FUV component is actually about 20× that of the X-rays. This suggests that it is unlikely to originate from the steep potential well near a collapsed object either because the emitted radiation would be nearly monoenergetic. On the other hand, the three spectral chracteristics we have noted, the panchromatism, dominance in the FUV, and possible emission in hydrogen lines are all characteristics of White Light Flares on the Sun. These flares are thought to be the reaction of the chromo-/photosphere by magnetically guided electron/ion beams, causing marginal heating of the irradiated photosphere. From the standpoint of X-ray flaring and panchromatic rapid flux variability, magnetic flaring must once again be considered as a possible mechanism. A final, important argument for

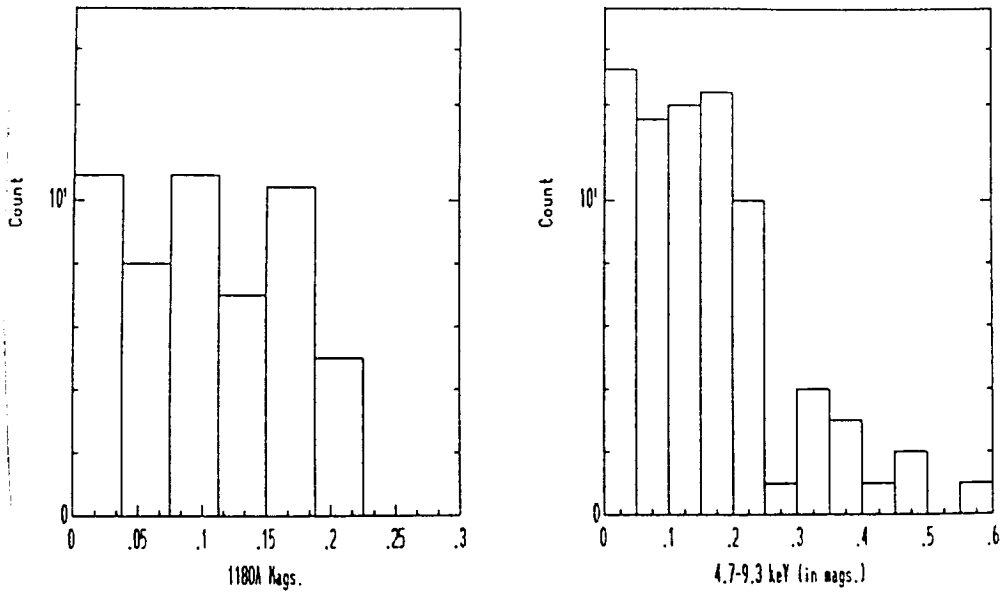

Fig. 6 – Histogram comparison of rapid FUV and X-ray flux variations of γ Cas.

To compare the FUV with the X-ray variations, we performed the same histogram analysis on the mean fluxes of consecutive orbits from the Parmar et al. (1993; *Exosat*; 5-9 keV) dataset in Figure 6b and the Horaguchi et al. (1993; *Ginga*; 1-9 keV) data (not shown). The FUV and X-ray distributions are nearly identical in shape and magnitude threshold. Further investigation shows that the histogram form holds for data grouped even 0.5 hr apart. In view of these similarities, we suggest that the FUV and X-ray variabilities have the same origin.

What could this origin be? The energy of the fluctuating X-rays is too high for them to arise from gravitational potential energy on the surface of the Be star. The energy in the FUV component is actually about 20× that of the X-rays. This suggests that it is unlikely to originate from the steep potential well near a collapsed object either because the emitted radiation would be nearly monoenergetic. On the other hand, the three spectral chracteristics we have noted, the panchromatism, dominance in the FUV, and possible emission in hydrogen lines are all characteristics of White Light Flares on the Sun. These flares are thought to be the reaction of the chromo-/photosphere by magnetically guided electron/ion beams, causing marginal heating of the irradiated photosphere. From the standpoint of X-ray flaring and panchromatic rapid flux variability, magnetic flaring must once again be considered as a possible mechanism. A final, important argument for

extra

the Be star origin of this activity is the observation of rapid variations along the V, R emission components (including fine structure). This suggests that different sectors of the overlying plasma are excited by several transient hot sources *close* to the Be star. In our view it becomes increasingly difficult to maintain the degenerate binary hypothesis in light of these new observations.

Finally, we may turn to a number of optical photometric reports of sudden brightenings on a 1-2 day timescale in other Be stars, most recently κ CMa (Balona 1990) and ϵ Cap (Balona 1993). These reports tend to corroborate earlier visual reports of sudden, several-minute optical brightenings of HD160202 (Bakos 1970) and 66 Oph (Page and Page 1970). It would appear that magnetic flaring should be considered as the most likely single mechanism responsible for each of the aperiodic activity outlined in the foregoing (cf. Underhill and Fahey 1984).

This work was supported by NASA Contracts NAS5-31221 and P.O. S-97229-E.

References

Auer, L. H., and Mihalas, D. M. 1972, ApJS, 24, 293.
Bakos, G. A. 1970, S&T, 40, 214.
Balona, L. A. 1990, MNRAS, 245, 92.
Balona, L. A. 1993, ed. G. Peters, Be Star Newsletter, No. 26, p. 5.
Blondel, P. F., Televera, A., and Djie, H. R. 1993, AA, 268, 640.
Horaguchi, T. 1993, PASJ, 46, –.
Hubeny, I. 1988, Comp. Phys. Commun., 52, 103.
Page, A. A., and Page, B. 1970, Proc. Astr. Soc. Aust., 1, 324.
Parmar, A., Israel, G. Stella, L, and White, N. 1993, AA, 275, 227.
Peters, G. J. 1982, PASP, 94, 157.
Peters, G. J. 1986, ApJ, 301, L61.
Slettebak, A., and Snow, T. P. 1978, ApJ, 224, L127.
Smith, M. A. 1989, ApJS, 71, 357.
Smith, M. A., and Polidan, R. S. 1993, ApJ, 408, 323 ("SP93").
Smith, M. A., Peters, G. J., and Grady, C. A. 1991, ApJ, 367, 302, ("SPG91").
Smith, M. A., Peters, G. J., and Grady, C. A., and Feigelson, E. D. 1993, ApJ, 409, L49.
Smith, M., Hubeny, I, Lanz, T., and Meylan, T. 1994, ApJ, subm.
Underhill, A. B., and Fahey, R. P. 1984, ApJ, 280, 712.
Yang, S., Ninkov, Z., and Walker, G. 1988, PASP, 100, 233.

DISCUSSION

BALONA - Supposing your slabs are concentrated over a much wider area, or you have a grand slab covering 20-30% of the stellar disk. Then you will not observe a dimple but rather a much broader line profile variation like that hypothesized for an $l = 2$ NRP mode. Can you comment?

SMITH - Dimples have a smaller characteristic width than the global *lpv*'s from

an NRP $l = 2$ mode. It is unlikely that several slabs could "conspire" to emulate a profile shape from this mode, and far less likely still that they would do so over the many profiles that the global $l = 2$ distortion has been documented. However, it is possible at times that a few dimples could be confused with bumps from Penrod's $l = 8$ mode.

OWOCKI - You mentioned that dimples appear mostly at line center, but wouldn't your "slabs" also appear off disk center and thus away from line center. The one episode you did mention that appeared from line center you interpreted in terms of a falling slab, but couldn't this just be a slab off disk center?

SMITH - The preference for observing dimples near line center is probably simply a signal to noise issue. On your second point, slabs can't have vertical velocities larger than the line width for the Smith-Polidan scattering mechanism to work, so they are basically doppler imaged from the disk to the profile. Thus one can discriminate between slabs having vertical velocities and their being situated near the equatorial limbs. In particular, inverse P-Cygni dimples arise from an unequal distribution of scattered photons toward the "East" and "West" edges of the penumbra. This is an indicator that the slab is moving relative to the surface.

KOUBSKY - Could you comment about the visibility of "dimples" in Hα profiles?

SMITH - Some evidence for sympathetic dimples in Hα is presented by Smith (1989). But beyond these changes in shape, I think it may be possible for dimples to affect the line's EW. That is, if the Hα source function is high enough, incipient transient emission might be observable.

PRINJA - In your slab model for λ6678 "dimples," you described a weakening of the C IV λ1550 doublet. Can you comment further on how this diagnostic relates to the slab model, and also on whether the velocity range over which profile changes in these lines is consistent?

SMITH - This interpretation (see Smith and Polidan 1993) rests upon the NLTE work done by Pauldrach which suggests that when C IV lines are formed in a plasma denser than 10^{11} cm^{-3} the ratio of level departure coefficients, and hence the lines' source functions, greatly increase. This causes the C IV doublet to weaken. The slab densities we estimate are consistent with the line of sight going through plasma with this higher-than-nominal density. I found little velocity information in the IUE profiles of C IV; the variations are certainly consistent with profile changes at low velocities.

LAFON - Can your slab interpretation be considered dynamically consistent with what is known about the magnetic field of this star?

SMITH - I would have to say we don't know anything about real field strengths or configurations on λ Eri. As far as dynamical model descriptions, they are still being formulated and debated even for the Sun!

WAELKENS - The dimples you observe are reminiscent of those seen in β Pic, another star surrounded by a gas disk. The interpretation in that case is infall by comets. In your observations you show evidence of infall, not outflow of the "dimpling" material. Could you comment on this? Also, yesterday we learned that shocked-infall can generate X-rays. Why didn't you mention that this is a possible energy source for the λ6678 line emission?

SMITH - True dimples develop in tens of minutes and show flanking emission wings. As I understand it, the β Pic features you are referring to are absorptions, only, and develop over a timescale of a day. Moreover, dimples seem to be anticorrelated with the presence of a disk or emission activity in λ Eri. I agree that infall onto the star could generate X-rays (or emission in Hα or He I lines). However, my point is that the emission that is observed is greatly in excess of what can be produced by the matter in the circumstellar disk, assuming that it were all to fall back to the star. It is the column density for the mean depth of formation of the λ6678 line which now gives us a good handle on the heating requirements, and it's too much for the CS matter available.

KOGURE - I would like to ask you a question about X-ray emission from γ Cas. Murakami *et al.* showed a rapid variability of a timescale of 10 sec and attributed this to a white dwarf. Similar rapid variability was also observed with *Ginga* (Horaguchi et al. 1993). Can rapid X-ray variability originate from magnetic flaring activity?

SMITH - The thesis of my talk is, yes, I think so. The chain of reasoning I make is, first, that the FUV rapid variability shows a spectral distribution like a B star's and thus can originate in the Be star's photosphere and, second, that the FUV and X-ray show similar temporal characteristics. Taken together, these facts suggest that the X-ray variability originates there too. I suggest a picture like that of solar White Light Flares, which appear to originate from particularly energetic beams of electrons or ions induced by flares. These penetrate deep into the Sun's chromosphere or photosphere where they can elevate the temperature of high density plasma only slightly. As for the timescale of the X-ray variations, they show chaotic behavior, which means there is no characteristic timescale over a range from $\sim$10 sec to $\geq$90 minutes, perhaps longer. The neutron star advocates have attempted to use 10 sec as a diagnostic for infall into a n.s. potential well, but this is not correct if there is no special timescale. The white dwarf picture has the problem of requiring a rather high mass loss rate. I think that each of these pictures suffers from these problems, though they probably can't be ruled out.

PUZZLING PROBLEMS OF He I LINE FORMATION IN EARLY B STARS

MYRON A. SMITH,
IUE/CSC Observatory, 10000A Aerospace Rd., Lanham-Seabrook MD 20706, USA

and

IVAN HUBENY, AND THIERRY LANZ
Goddard Space Flight Center, Greenbelt, MD 20771, USA

1. Introduction

Although NLTE model atmospheres have been shown to resolve most of the equivalent width (EW) discrepancies for blue He I lines (Auer and Mihalas 1972, 1973), Wolff and Heasley (1984, 1985) have demonstrated that discrepancies remain for the leading members of the singlet/triplet 2P – nD series, *viz.* λ6678 and λ5876. These two lines are the strongest nonresonance He I transitions and are important because they respond to thermal changes in the superficial atmosphere ($\tau \sim 10^{-3}$) of early B stars. In order to understand the observed rapid variations of the λ6678 line in mild Be stars, we undertook a survey of EWs of λ6678 and λ4388, namely the first and third member of the same series. These two lines have a log gf ratio of 15 but have similar EWs in B star spectra. Our new observations confirm the red line discrepancy noted by WH85 and point to additional EW differences among various groups of B stars not noted hitherto.

2. Observations and Models

Observations were conducted at the McMath Solar telescope using a resolution of 50,000 and 30,000, respectively, for the red and blue line. We observed 100 chemically normal B0.5-B5 stars known not to have obvious secondary contamination. We converted their published *uvby*Hβ colors to (T_{eff}, log g) from WH85's calibration, and when necessary the WH85 Hγ profile criterion to determine log g's.

We used the TLUSTY code (Hubeny 1988) to compute pure H/He NLTE model atmospheres and line profiles. These models include 14 discrete singlet and triplet He I levels plus one for the He II ground state; additional He II states are unimportant for T_{eff}'s < 30,000K. Profiles computed with various ξ_t values showed negligible difference in EW. *Figs. 1* and *2* show our observations against the models of AM73 and TLUSTY. Because Be stars with emission have contaminated photospheric EWs, these stars are omitted in the following discussion.

L. A. Balona et al. (eds.), *Pulsation, Rotation and Mass Loss in Early-Type Stars*, 273–274.

3. Results

λ4922 shows good agreement between EWs predicted by AM73, TLUSTY, and our data – nor do λ4922 EW differences exist among subgroups, except that giants are predicted/observed to show 250mÅ EWs than dwarfs. Yet as *Fig. 1* shows, while there is agreement between predictions from the two codes, their predictions fall short by ∼100mÅ of the observations. Also, contrary to theory, the EWs of giants are stronger than B dwarfs. Finally, EWs of known pulsating B stars, and Be stars without strong emission (at obsn.) are all larger than for B dwarfs.

The intergroup EW differences for λ6678, but not for λ4922, is a new result. We have tried to model these differences with a variety of toy model atmospheres with modified ρ, T distributions, including dense slabs. None of these can enhance the λ6678 EW without also influencing λ4922 and disturbing its agreement. To resolve this conflict, we are currently building a new generation of model atmospheres with blanketing by $\sim 10^6$ lines. This will include investigation of the influence of raised microturbulence in pulsating and Be star atmospheres.

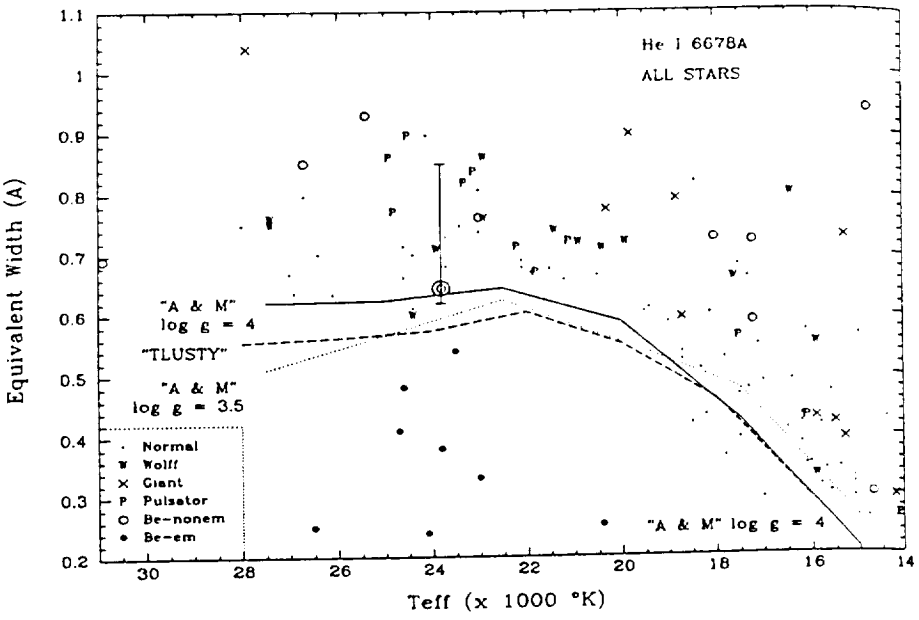

Figure 1 – Plot of predicted/observed EWs for λ6678. (EW range of λ Eri noted.)

References

Auer, L. H., and Mihalas, D. M. 1972, ApJS, 24, 293.
Auer, L. H., and Mihalas, D. M. 1973, ApJS, 25, 433, ("AM73").
Heasley, J., Wolff, S, and Timothy, G. 1982, ApJ, 262, 663.
Hubeny, I. 1988, Comp. Phys. Commun., 52, 103.
Wolff, S., and Heasley, J. 1985, ApJ, 292, 589, ("WH85").

THE ASTROPHYSICAL JOURNAL, 408:323–336, 1993 May 1

DYNAMIC PROCESSES IN Be STAR ATMOSPHERES. I. "DIMPLE" FORMATION IN THE He I λ6678 LINE OF λ ERIDANI

MYRON A. SMITH
CSC/*IUE* Observatory, Science Programs, Computer Sciences Corporation, 10000-A Aerospace Road, Lanham-Seabrook, MD 20706
AND
RONALD S. POLIDAN
Laboratory for Astronomy and Space Physics, Goddard Space Flight Center, Greenbelt, MD 20771
Received 1992 May 27; accepted 1992 October 27

ABSTRACT

"Dimples" are ephemeral absorption features flanked by incipient blue/red emission in the He I λ6678 line profiles of λ Eri and several similar mild classical Be stars. They develop rapidly (~15 minutes), last 2–4 hr, and are observed in this line on the average at least once per night, making them the most ubiquitous of the "spectral transients" appearing in the line profiles of at least some mild Be stars. Their formation may well be related to the unknown instability-causing mass-loss episodes in Be stars.

In this paper we discuss simultaneous *IUE* and optical (λ6678) time-serial observations of λ Eri, together with near-simultaneous UV continuum observations made by *Voyager 1*, in 1990 October. We find several examples of weakenings of the C IV, N V resonance lines that coincide with the appearance of λ6678 dimples. The absence of variations in other UV lines and in the UV continuum at the same time (*IUE*) or nearly the same time (*Voyager*) argues against dimples being caused by thermal variations from the underlying star. We suggest instead that the resonance line weakenings are caused by non-LTE effects associated with the condensation of high density structures at some elevation over the star. We present a simple model of an opaque (in the line only), essentially stationary slab which backscatters λ6678 line radiation into a surrounding "penumbral" region. λ6678 photons are scattered a second time in this region back into the observer's line of sight and in the process acquire the local projected doppler shift from rotation. We examine several attributes of this mechanism and find that slabs typically have a projected radius of about 1 $R_\odot$, an elevation of $\sim 0.10 R_*$, and a density of $\sim 2 \times 10^{11}$ cm^{-3}. Our models can also match dimples resembling "P Cygni" features by permitting our model slabs to rise or fall and at the same time to move retrograde or prograde with respect to the stellar surface. Slabs would probably produce too little emission to be easily detected in the Hα profile. Their detection in strong He I lines seems the best stategy among early Be stars.

Slabs contain enough mass ($> 10^{-14}$ $M_\odot$) and develop over such a large area and so rapidly as to greatly limit the number of mechanisms that could form them. Their rapid development spatially over the star precludes a purely thermal origin, e.g., from the propagation of a shock at the speed of sound. Yet, in terms of bulk motion dimples represent an exclusively low vertical-velocity phenomenon. Arguments can be advanced that dimples are not the results of ballistic tossings of blobs or of orbiting circumstellar ejecta. One viable mechanism for their formation requires that dimple-slabs condense from ambient rarefied material via a supersonically propagating instability. If this velocity is understood in terms of an Alfvén wave, a case can be made that magnetic fields of ≥100 G can exist in small regions above λ Eri and many other mild classical Be stars.

Subject headings: line: profiles — stars: emission-line, Be — stars: individual (λ Eridani) — ultraviolet: stars
ultraviolet: stars

1. INTRODUCTION

Classical Be (early-type, post-ZAMS, putative single) stars are unrivalled among main-sequence variable stars for their abrupt episodes of mass loss after extended periods of dormancy and for their spectroscopic variability on time scales from minutes to decades. The physical cause(s) of the "Be phenomenon" is not understood at all. One assumes that the rapid variability (minutes to days) is related to the basic mass-ejecting instability. The tools needed to study rapid activity became available only in the 1980's with the advent of stable silicon diode arrays and the availability of the *IUE* satellite, which permitted coordinated ground/space observing campaigns. Progress has proceeded unabated in the meantime on the structure and evolution of their circumstellar ejecta, generally regarded as disks. For example, the long-term nature of Hα "*V*/*R*" variability in circumstellar envelopes has long been documented by photographic studies and more recently in spectra obtained with diode arrays. The physical characteristics of circumstellar structures that are produced by past outbursts can be elucidated by simple models applied to a combination of IR, millimeter-wave, polarization observations (e.g., Waters et al. 1991; Waters & Marlborough 1992). In addition, ingenious mechanisms for the maintenance of these disk structures (Lamers & Pauldrach 1991; Bjorkman & Cassinelli 1992) have been advanced. However, invariably these rely upon an unknown deus ex machina for the initial ejection for otherwise the disklike structures that these models attempt to explain would be permanent and static.

In this series of papers we will address the dynamics of Be star atmospheres with the goal of defining the physical characteristics of unstable regions associated with rapidly variable spectroscopic signatures and nonthermal radiation in at least

some classical Be stars. In this paper we begin with a simple ad hoc mechanism to explain a common phenomenon, the appearance/disappearance of features resembling "dimples" in the λ6678 He I line profile of the prototypical mild, rapidly rotating ($V \sin i = 310$ km s^{-1}), nearly edge-on B2e star, λ Eri (Smith, Peters, & Grady 1991). Mild Be stars do not show emission in their He I or Balmer lines most of the time. Their He I lines peak in strength at types B1–2 and are generally formed in or near the photosphere. If the $T_{\rm eff}$ is much cooler, the ultraviolet flux that can excite 21 eV transitions in circumstellar plasma is limited. If any hotter, the stellar radiation field shifts the ionization to He II. As the strongest nonmetastable excited transition in the He I atom, the λ6678 line is the ideal optical line to monitor upper atmospheric conditions of B stars and to test for differences in formation from other lines formed near the continuum. We have previously exploited this property and cataloged a rich variety of variability patterns that we designated as "spectral transients" (Smith 1989, hereafter S89). We defined transients specifically for the λ6678 line as any statistically significant emission or absorption event that appears and then decays over minutes to hours and which is not associated with predictable behavior, such as nonradial pulsations. In most cases spectral transients can be placed in discrete phenomenalogical classes, e.g., *types a-d*. Among these the "dimple transient" (*type b2*) is by far the most common.

Our basic definition of a dimple in the λ6678 profile is the unexpected appearance of central 2–3 Å wide cusp-shaped absorption flanked by incipent emission. The emissions and absorption attributes cancel so that the line strength (equivalent width) remains constant to within measurement errors ($\sim$ 10%–20%) of the distorted profile; this point will be developed further below. Figure 1 is a textbook example of a typical dimple, with the central absorption and flanking emissions labeled. The profile is contrasted with an "immaculate" (no-dimple) profile and compared to a model fit discussed below. The feature typically lasts 2–4 hr as it grows from and decays back to a smooth underlying profile. An average dimple shows an absorption cusp 1½% deep, and the absorption and emission components each amount to about 2.5% of the line's equivalent width. Dimples tend to show a slight movement to the red associated with rotational advection. However, their short lifetimes generally prevent a check against their expected acceleration from the star's rotation. We will exhibit several examples of dimples and list other stars in which they may have been recently observed.

In this paper we show that ultraviolet spectra generally show line strength changes when λ6678 dimples first appear. This correlation will lead us below to a simple ad hoc picture that requires photon scattering and Doppler-mapping them onto a rotating stellar disk. We will constrain this description further in a subsequent paper detailing more extensive NLTE model atmosphere computations than discussed herein as well as simultaneous observations of dimples forming in different He I lines.

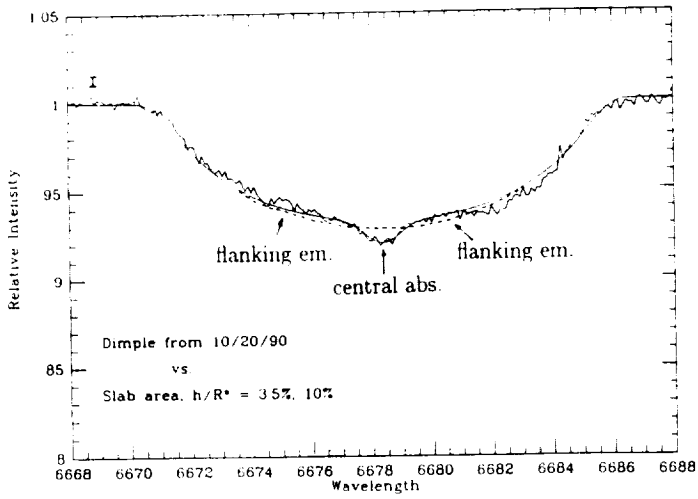

FIG. 1.—"Textbook" example of a dimple in the λ6678 profile of λ Eri with the "central absorption" and "flanking emissions" indicated. The dimple observation was made at 12:23 UT on the date indicated. The smoothed lines show a fit to the observations according to the "slab" model discussed in the text. The slab area and elevation values indicated and with the slab placed at the observer's substellar point. The dashed line indicates the computed rotation-only profile. The poorer fits far from the dimple absorption/emission result from a periodic variability probably due to nonradial pulsation. Error bars are photometric errors inferred from deviations in the continuum.

2. DIMPLE ATTRIBUTES

The definition of dimples in line profiles is restricted so far to the λ6678 line alone. In S89 we used the term dimple to describe a rather well defined spectroscopic apparition which can be modified only slightly from new observations. Continued monitoring of λ6678 in λ Eri since S89 has clarified several characteristics of dimples that were not clear at that time. We describe these briefly as follows:

First, typically a dimple may appear on average every few hours. Occasionally, however, two or even three can appear at about the same time, suggesting that they are caused by a common local instability. Figure 2 shows an example of three dimples that appeared together. These and several other figures use data obtained from our long-term monitoring program on λ Eri using the "solar-stellar" McMath/CCD system over the last few years. None of these features was clearly visible 10 minutes earlier. In some cases there can be ambiguity, but here both emission *and* absorption occurs

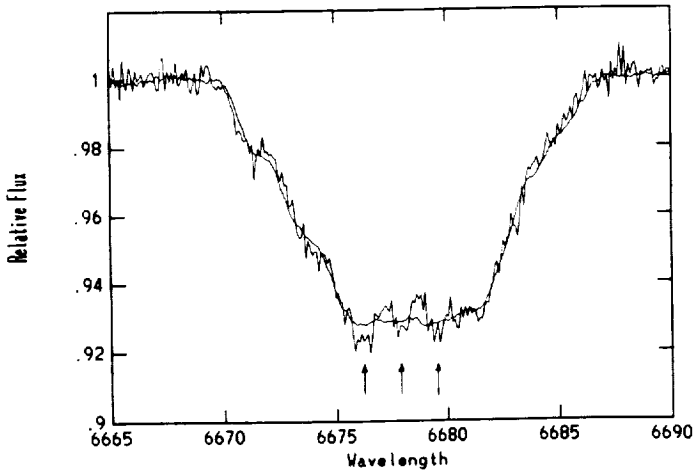

FIG. 2.—Simultaneous appearance of three "dimples" (arrows) in the λ6678 line of λ Eri (CCD observations) at 4:57 UT on 1991 March 17. The smoothed (over six points) profile represents the predimple profile obtained ten minutes earlier, at 4:47 UT; because the observation was featureless, the smooth line conceals no essential information. The full development of these dimples was followed in our observations but is not shown.

simultaneously to conserve the equivalent width so we consider this interpretation likely. We have found six to eight other examples of pairs of dimples appearing together within the observational sampling frequency of 5–10 minutes.

Second, in contrast to the S89 discussion, it is now firm that dimples can appear on the edges of profiles. The reason we have modified this view is that we have come to appreciate how difficult it can be to classify features in the wings as dimples. A very high signal to-noise ratio is needed to detect incipient emission in these cases. Figure 2 shows one example of a dimple in the (blue) wing. In this case it was not clear that this "absorption" is a dimple until several subsequent spectra could be averaged and the feature compared.

Third, as in S89 we believe that dimples may also form when Balmer and He I lines exhibit emission. However, we have noted extended periods when the frequency of dimples decreases to nearly zero. These periods coincide with rapid micro-emissions in the core of the line (Smith 1991). The frequency of dimples may also vary on time scales of a few months, for example, being high during 1990–1991 when the line strength (equivalent width) was strong and being low during and just following Hα emission episodes.

Fourth, S89 characterized pure absorption stationary transients as "*type d*" events. Since these events show no emission the equivalent width increases from the temporary absorption feature alone. However, rather than *type d's* representing a separate phenomenon, these features may well represent a related class of dimples (low-altitude "slabs"). We will develop this point in § 4.4.

Fifth, highly time-resolved observations show that dimple formation is characterized by a changing dimple profile which starts out as a very narrow feature (rivaling the instrumental profile) which broadens while developing flanking emission. In contrast, dimples fade by weakening uniformly. Figure 3 shows two examples of a few available of the initial stages of a dimple's development. At the risk of underrepresenting real profile variations, we will economize figure space and refrain from following the full dimple evolution that the data sequence shows. Indeed, the second case depicted is the beginning of one of the strongest dimples we have ever observed. Clearly, these dimples change their shape by broadening as they grow. It is a reasonable assumption that their initial formation as a narrow (typically 8–10 km s^{-1} wide, but this is comparable to our instrumental resolution) feature represents the optically thin stage of a developing dimple. From the examples depicted, this development to optical thickness lasts only ~15 minutes.

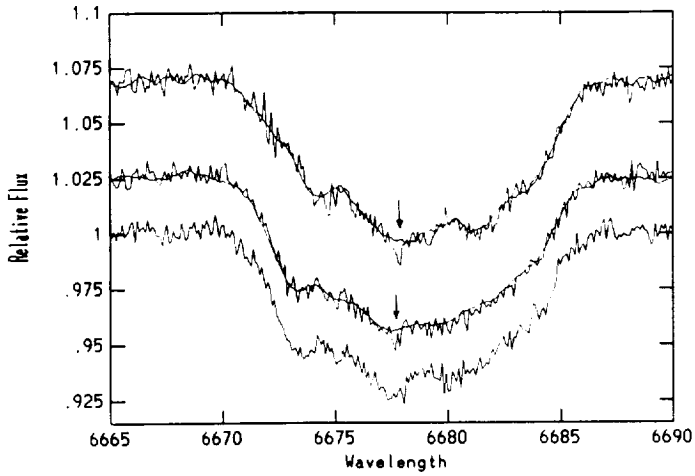

FIG. 3.—The development of two dimples on the dates shown (*arrows*). In each case the solid line is the smoothed previous observation obtained ~15 minutes earlier. Note that the dimples' initial development is marked in each case by a narrow absorption feature. The times of the observations are (*upper pair of smoothed and unsmoothed curves*) 1990 October 22 at 12:05 and 12:17 UT; and (*middle pair and lower curve*) 1991 January 18 at 8:41, 8:59, and 9:06 UT.

In Table 1 we exhibit equivalent width statistics of pre-/during-/post-dimple observations profiles on those nights for which dimple observations are exhibited in this paper. In each case the table lists the means and sigmas in mÅ of a 5 Å strip centered on the active dimple in the profile over 1–2 hr. The last column gives the composite deviation (emission plus absorption) of the dimple from the mean pre-dimple profile. Since a dimple generally extends for no more than 6 Å, nearly all the profile activity is included in these measurements. Table 1 shows that the percentage difference between pre- (or-post-) dimple and dimple profiles occasionally exceeds 30% of the composite deviation, but is ≤10% most of the time. From these statistics we conclude that the dimple composite equivalent width is constant during its evolution to measurement errors, which to be conservative we will adopt as 10%–20% of the composite dimple strength. (The exception is that at the beginning of the dimple the equivalent width shows a "momentary" increase of about this measurement error.) The conservation of equivalent width of the λ6678 line during the development of dimples is a major underpinning of our proposed mechanism for the dimple phenomenon.

A reconnaissance of 45 nights of our 1988–1991 data base on λ6678 profiles from λ Eri suggests a frequency of occurrence of about 1.3 ± 0.3 per 7 hr night. The uncertainty here arises from a limited time sampling on a given night determining whether a narrow absorption feature is part of a true dimple. Some 2/3 of all transients are dimples or related *type d* events.

In order to establish that dimples are not a peculiarity of the spectrum of just one Be star, we have searched for dimples in the λ6678 lines of other B stars while undertaking a general He I line survey. Table 2 lists five stars for which multiple spectra reveal dimple-like features and a smooth profile an hour earlier/later. To qualify for inclusion into this table, our candidate dimples have had to adhere to the defining characteristic: concomitant absorption/emission with a constant equivalent width. Inspection of Table 2 shows that the dimple phenomenon in λ6678 may extend from types B1 through B5. Note that all these stars exhibiting dimple profiles have $V \sin i \geq 250$ km s^{-1}. We also point out that one of the stars listed, HR 1023, is not known to be a Be star. P. Avellar of the National Solar Observatory has monitored the Hα profile of this star since the discovery of its probable dimple in 1991 November and has found no emission.

3. RESULTS: THE ULTRAVIOLET-DIMPLE CONNECTION

3.1. *IUE and McMath Data*

Until responses could be found in other spectral lines, a physical interpretation of dimples has been difficult because of their unpredictable occurrences and short lifetimes. The most natural of these to look for is an evidence of heating in the ultraviolet. We were able to arrange scheduling three nights of simultaneous coverage on 1990 October 21–23 (UT) with the *International Ultraviolet Explorer* satellite and the CCD solar-stellar spectrograph at the McMath Solar Telescope. We

TABLE 1

EQUIVALENT WIDTH STATISTICS FOR SEVERAL DIMPLES (5 Å BANDPASS)

Date	Dimple/Post-/Pre-	Equivalent Width (mÅ)	Equivalent Width-Sigma (mÅ)	Aggregate Dimple Strength (mÅ)
1990 Oct 21	Dimple	382	4	19
	Post-	373	4	19
1990 Oct 22	Dimple	354	7	23
	Post-	354	5	
1990 Oct 23	Dimple	357	11	11
	Post-	361	5	
1990 Oct 23	Pre-	375	4	
	Dimple	379	4	19
	Pre-	380	5	
	Dimple	383	3	13
	Pre-	381	4	
	Dimple	377	3	11
	Post-		3	
1991 Jan 5	Pre-	376	3	
	Dimple	360	3	20
1991 Jan 18	Pre-	346	4	
	Dimple	343	3	20
1991 Mar 17	Pre-	358	4	11
	Dimple	361	...	
Averages	Pre-/Post-	367	5	
	Dimple	368	5	16
Sigma of mean			4	

monitored λ Eri continuously over three consecutive 8 hr US2 shifts on these dates using the large aperture, high-dispersion mode with the short-wavelength camera. The SWP sequence numbers for these *IUE* observations are 38872 – 84, 38891 – 39905, and 39911 – 24. Cycling for data readouts and camera preparations limited our time resolution to 30–35 minutes. Integration times of 1 minute were used to optimize exposures in the $\lambda\lambda$1350–1550 region. For the $\lambda\lambda$1548–1550 C IV doublet and other features of interest, we found the internal errors in equivalent width (EW) measurement to be about 4%.

The McMath observations were made as nearly simultaneous with the *IUE* shifts, except that the first half of October 21 was clouded out. We used the same instrumental set-up described in S89. This configuration gives a wavelength sampling of 95 mÅ, a spectral resolution of 42,000, and a sampling frequency of 6–8 minutes (lengthened to 10 minutes at high air masses). The resulting signal-to-noise ratio is ~300, as measured by spectrum-to-spectrum flux deviations at a given pixel. Except for an occasional "cosmic ray", the pixel fluctuations showed no fringing, flat-fielding flaws, or significant deviations from Gaussian statistics (cf. Smith 1989). The data were reduced, plotted, and equivalent widths measured in IRAF.

The *IUE* spectra were reduced at Goddard using standard RDAF/*bin* and *feature* routines to measure fluxes, equivalent widths, and wavelengths in a consistent manner. Peters (1991) has shown that the fluxes of λ Eri and related Be stars can be measured with the SWP large-aperture configuration to an internal (spectrum-to-spectrum) accuracy of a few percent. We have followed Peters' convention of measuring integrated fluxes in the $\lambda\lambda$1425–1475 band. We also measured fluxes at the 20 Å band centered at λ1195 ("λ1200") with similar trends as the λ1450 data. The λ1200 fluxes averaged 5.46 ± 0.03 10^{-10} ergs cm^{-2} s^{-1} Å^{-1} on the first two nights and brightened by 18% on the third. The λ1450 continuum flux averaged 14.3 in the same units and showed somewhat smaller spectrum-to-spectrum flux excursions. We exhibit the λ1200 fluxes in Figure 10 below because we anticipate that these would be the more sensitive indicator of any high temperature transients on the star. Some trends were found in these fluxes over the 8 hr shifts. For example, the continuum slope on October 22 was consistent with the higher level on October 23. No significant rapid variations occur during the shifts and particularly none that could be coincident with the λ6678 dimples. This would indicate that photospheric heating is not the mechanism responsible for the formation of dimples.

TABLE 2

STARS SHOWING POSSIBLE 6678 Å DIMPLES

Star	Spectral Type	$V \sin i$(km s^{-1})
HR 1011	B5 V	244
HR 1423	B1 Ve	340
56 Eri	B2 Ve	240
120 Tau	B2 Ve	271
8 Lac	B2 Ve	348

In addition to the UV continuum, we measured equivalent widths for lines of several ions: He II (λ1640), Si II ($\lambda\lambda$1527–1533 doublet), Si III ($\lambda\lambda$1294–1303 system), Si IV ($\lambda\lambda$1395–1403 doublet), C III (λ1247), C IV ($\lambda\lambda$1548–1550 doublet), and N V ($\lambda\lambda$1239–1243 doublet). Except for C IV and N V, we found no variations in these lines' equivalent widths. Having an equivalent width of 1.9 Å on the first night, the C IV line showed a 17% larger equivalent width on the second night.

In Figures 4–6 we summarize several of the equivalent widths and fluxes for each date, normalized to their nightly averages. The normalized 1200 Å fluxes and equivalent widths of He I λ6678 (shifted upward by 15%), He II and C III show

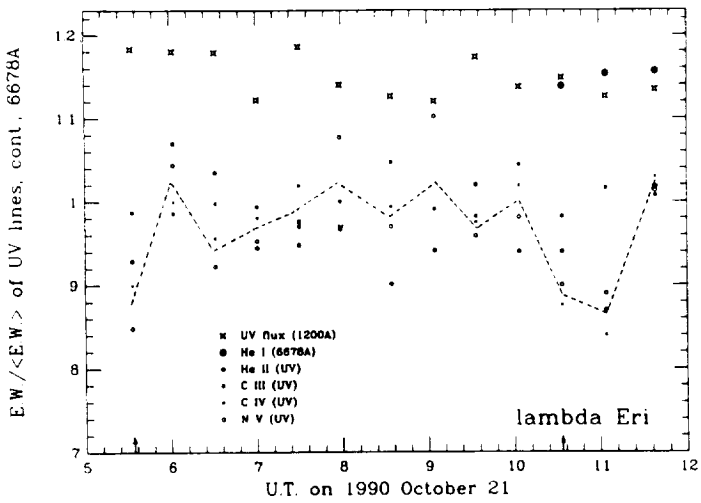

FIG. 4.—Normalized equivalent widths (EWs) of *IUE* high-dispersion spectra on October 21. UV continuum and λ6678 strengths are uniformly shifted upward 15% to avoid confusion. The means of the variations of the C IV and N V lines are shown as dashed lines in this and the following two figures. The first observation shows a "recovery" of C IV, N V resonance line strengths (*crosses, circles*). Another line-weakening event also is evident at 10:30–11 UT. The C III λ1247 (*squares*) and He II λ1640 (*small dots*) show no credible variations, nor do the (upward displaced) *IUE* λ1450 continuum fluxes and λ6678 EWs. We denote the appearances of dimples with arrows; Fig. 7 corresponds to the second of the two C, N line weakenings shown here.

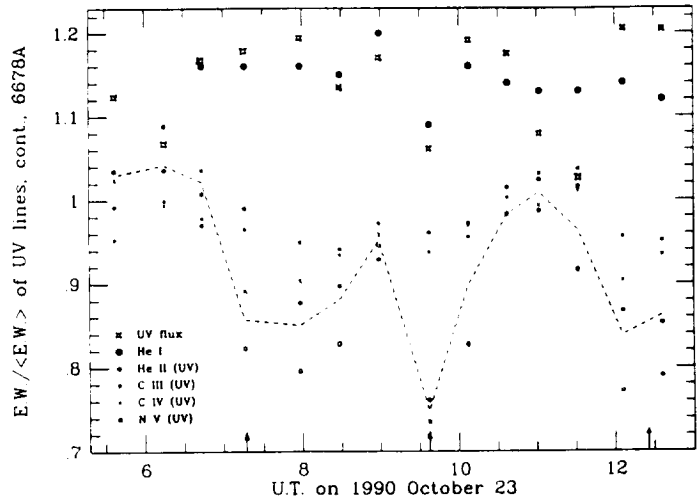

FIG. 6.—Normalized EWs from *IUE* observations on October 23 (same symbols as for Fig. 4). UV continuum and λ6678 strengths are uniformly shifted upwards 15% to avoid confusion. The C IV, N V resonance lines show clear weakenings at 7–8, 9:30–10, and 12–13 UT. Note the dimples in Fig. 9 at these times (*arrows*).

uncorrelated fluctuations of a few percent. In contrast, the C IV and N V equivalent widths show correlated 10%–20% decreases generally lasting an hour or so at six different times when dimples appeared (*arrows in diagrams*). With one exception (a single dip in λ1640 strength at the end of October 23), we could not find any other UV feature which correlated with these sudden changes.

Although the overall λ6678 equivalent width showed no correlation with weakenings of the C IV and N V lines, we discovered that each of these weakenings coincided with the appearance several minutes earlier of a λ6678 dimple. We show five of these examples in Figures 7–9. Except when it occurs at the beginning of the night, we have tried to represent both the dimple and previous (nondimple) observation. In a few cases the λ6678 dimple appears to have preceded the first indication of a decrease in C IV, N V line strength by several minutes. Based on our statistics (five out of five dimple/C IV-weakenings), it is fair to conclude that the two spectral signatures are correlated and hence have a common origin. However, we did note a few were not accompanied by C IV line weakenings. This imperfect correspondence could be due either to the coarse time sampling of the *IUE* or to a difference in cloud sizes responsible for the He I and C IV variations. For example, if the C IV responds to a larger volume, as implied by their larger fractional changes in strength, we could be observing the outer region of the cloud *over* the stellar limb and the dense inner region, responsible for the He I, *against* the disk. In such a case the C IV might show a negligible change.

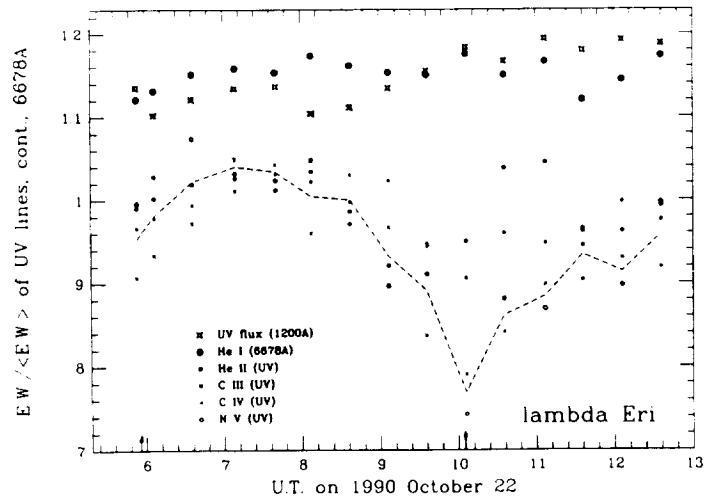

FIG. 5.—Normalized EWs from *IUE* observations on October 22 (same symbols as Fig. 4). UV continuum and λ6678 strengths are uniformly shifted upward 15% to avoid confusion. The C IV, N V resonance lines show a probable "recovery" at the beginning of the night and a clear weakening at 9–11 UT. Note the corresponding two dimples at the same times (*arrows*) in Fig. 8.

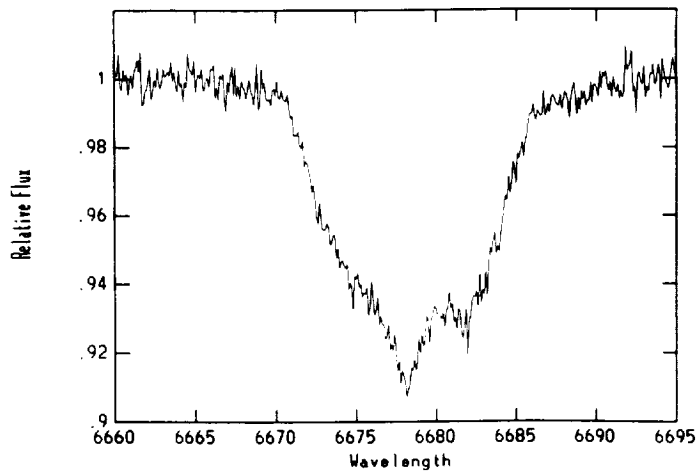

FIG. 7.—Dimple in λ6678 corresponding to the second UV resonance line weakening in Fig. 4. The dimple observation was made at 10:40 UT on 1990 October 21. As this was the first λ6678 observation of the night, there is no smoothed line depicting a pre-dimple profile.

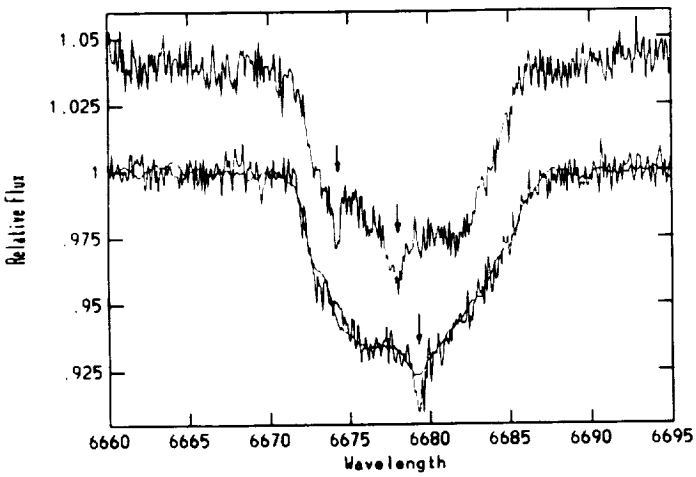

FIG. 8.—Two dimples followed by one dimple (*arrows*) corresponding to the UV resonance line weakenings in Fig. 5. A smoothed pre-dimple observation is shown, with a faithful rendition given to the core profile. The dimple observations were made on 1990 October 22 at 5:58 UT (*upper panel*) and 9:00 UT.

3.2. *Voyager Data*

Because the far-UV flux in a B star is quite sensitive to temperature variations between 25,000–150,000 K (Longo et al. 1989), we also obtained time with the *Voyager 1* spacecraft during the week of our McMath and *IUE* observations.

The *Voyager 1* Ultraviolet Spectrometer (UVS) observations covered the period from 1990 October 17–24. All observations were obtained in a high data rate mode with one spectrum obtained every 3.84 s. The *Voyager* UVS spectra cover the spectral region from 500–1700 Å, have a maximum sensitivity over 500–1200 Å, and have a resolution of ~15 Å (9.26 Å per channel). Analysis of the spectrophotometric data showed the B star continuum and no evidence of flux shortward of 912 Å. While *Voyager* UVS observations are in principle continuous, the drift of the star through (and out of) the field of view and incomplete ground station coverage produce gaps in the observations (see Polidan & Holberg 1987 for a discussion of the *Voyager* instrument and the observing technique). For the λ Eri observations discussed here we averaged 4–8 hr of continuous observation per day. These data were processed using standard *Voyager* data reduction methods with one added constraint: the 3.84 s spectra were combined into a series of "average" spectra with a temporal averaging of 12 minutes or less. This processing resulted in 69 independent spectra with integration times ranging from 207 to 715 s, with most having integration times in the 400–600 s range. The continuity of our data string was mainly limited by the availability of NASA's Deep Space Network of antennas. The resulting observing pattern prevented us from securing completely simultaneous *Voyager* coverage with our optical/*IUE* observations. Nevertheless, the statistics of occurrences and durations of "dimple-related" events seem secure enough to look for thermal signatures particularly shortward of 1000 Å, where any hot continuum source would be detectable.

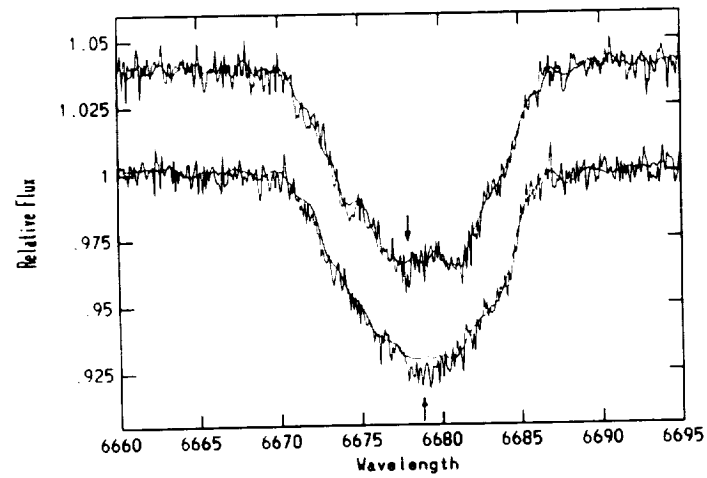

FIG. 9.—Two weak dimples corresponding to two of the UV resonance line weakenings in Fig. 6. The observations were made on 1990 October 23 at 7:11 and 9:41 UT. As in the previous figures, the pre-dimple observations are featureless, so the smoothed rendition retains all the essential information.

In order to test for continuum flux and shape variability we binned the *Voyager* spectra into three far-UV bands: a broad 930–1120 Å (λ1025) band and two narrower bands, 930–1000 Å (λ965) and 1050–1120 Å (λ1085). The former serves as a measure of the far-UV continuum flux whereas the latter to serve provide a color index. The λ1025 continuum measure and λ965/λ1085 color curves for 6 of 7 days are shown in Figure 10. Each of the points shown represents data binned from 1–3 hr. Experience with *Voyager* data suggests an rms errors of 3% in both fluxes and colors, consistent with the distributions shown. We have also surveyed the data over shorter time scales by binning the fluxes over several minutes. For the most part we find no statistically significant variability. Occasionally, the data show 1–2 σ decreases/increases in a $\frac{1}{2}$ hr time scale that affect clusters of typically three "points", representing $\sim\frac{1}{2}$ hr, in either λ965/λ1085 color or λ1025 flux, but never both at once. We regard these as fluctuations as statistically insignificant. In summary, like the simultaneous *IUE* fluxes described above, there is no evidence in our *Voyager* data of either decreases or increases in UV continuum fluxes over the time scales of dimples, 0.5–4 hr. One can show that this upper limit places a limit of a $\Delta T_{\rm eff} \sim 10{,}000$ K above the star's effective temperature for a "hot spot" having an area of the slabs we model below.

4. THE DETACHED DENSE-SLAB MODEL

4.1. *General Considerations*

In this section we will assume that the dimple forms from material initially above the star. We will consider and reject alternate mechanisms below that involve ballistic ejections, wind inhomogeneities, or orbiting remnants of a circumstellar disk.

It would be difficult to conceive of a mechanism for the formation of λ6678 dimples that does not require changes in gas temperature and density. Let us consider temperature changes first. The absence of enhanced UV flux when dimples occur, even though the C IV and N V resonance lines are affected, seems to rule out any substantial temperature elevations, e.g., to the $T_{\rm eff}$ of the underlying photosphere. Moreover, studies of the formation of the C IV line (Sakhibullin & van der Hucht 1983; Anderson 1985; Pauldrach, Puls, & Kudritzki 1986) suggest that C IV line strengths increase with the star's $T_{\rm eff}$. This dependence of C IV line strength on $T_{\rm eff}$ is also seen clearly in Peter's correlations of C IV strengths with periodic UV continuum modulations for λ Eri and other classical Be stars (Peters 1991, and private communication). These

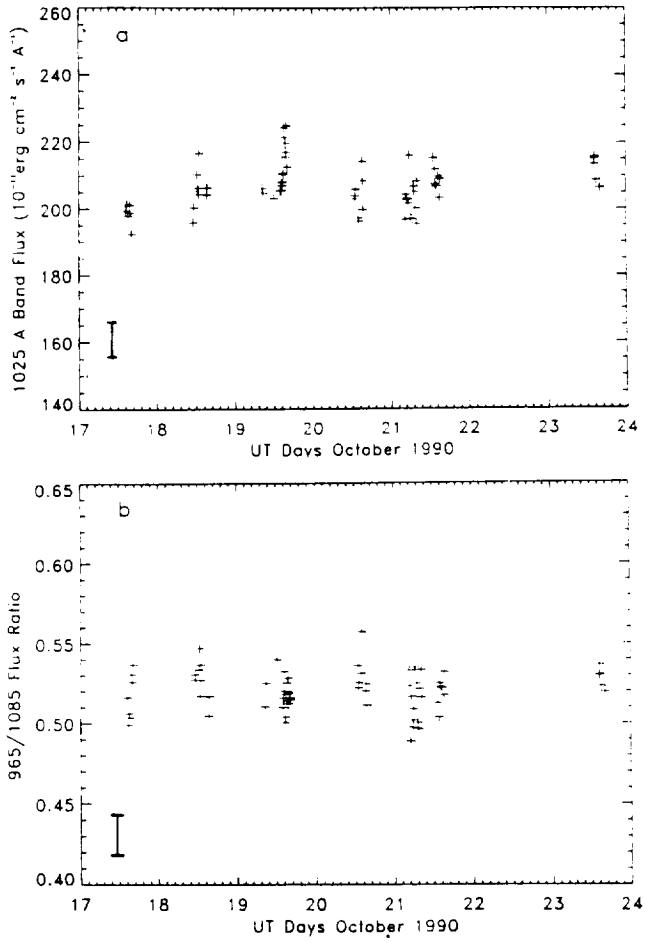

FIG. 10.—(*a*) *Voyager* broad-band 1025 Å light curve for λ Eri during the week of the *IUE* and optical spectroscopy. The data are individual fluxes taken from ≤ 12 minutes averages. Characteristic errors are $\pm 3\%$. (*b*) *Voyager* color curve formed by ratioing fluxes at 965 and 1085 Å bands corresponding to the 1025 Å fluxes in (*a*). Errors are the same as for individual fluxes.

correlations suggest that λ1450 continuum fluxes can be expected to increase at half the rate as C IV strength increases. Since the time-serial *IUE* data would have revealed UV continuum variations of 5%–10%, corresponding to the size of the observed C IV line decreases, the C IV decreases do not appear to be caused by cooled regions on the star's surface.

However, this consideration does not address temperature changes in the upper atmosphere material from which the dimple signatures form. If λ6678 were formed in LTE in superficial layers of the star's atmosphere it would be possible in principle to exclude heated material because the ionization shift toward He II would cause the column length to become very long in order for the λ6678 line to become opaque and form there. However, experiments with I. Hubeny's (1988) non-LTE code "TLUSTY" just as the final draft of our manuscript was being revised suggest an unexpected contrary situation. According to these new models, ad hoc elevations of the temperature lead to an overpopulation of lower He I atom states. Up to temperatures of at least 40,000 K this effect actually *increases* the density of ground-state λ6678 (2^1P) atoms so that the upper atmosphere becomes more, not less, opaque to this line (the effect is maximized for temperatures near 35,000 K). Consequently, hot as well as cool condensations must be included in one's consideration of how dimples form. However, our models indicate that this would have very little effect on continuum formation. It should be pointed out that in our Doppler-mapping models below we assume a "black" line core, but *broadened* intrinsic line profiles of essentially the same depth will produce the essentially same disk-wide flux profiles as long as the equivalent width of the intrinsic profiles is the same in the black and broadened profile cases. A minor caveat to this statement is that the third turbulent broadening parameter noted below may become unneccessary.

The short time over which dimples form suggests the formation region is small, that is that they form through local condensations. Theoretical considerations on the formation of the C IV and N V lines seem to support this conclusion. For instance, Pauldrach's (1987) integrated wind/atmosphere calculations show that the occupation levels of the ground states of these ions begin to diverage from LTE values at electron densities of $\sim 10^{11}$ cm^{-3} according to the only model available, with $T_{\rm eff} = 42{,}000$ K. The departure coefficients decrease to significantly below unity only when $N_e \leq 3 \times 10^9$ cm^{-3}. Indeed, for these densities the line effectively resonance scatters photons. Pauldrach's results, taken together with the λ6678 versus $\lambda\lambda$1548–50 correlation, suggests that λ6678 dimples could be caused by density perturbations injected (or collapsed) above the photosphere. We will refer to these density enhancements as "slabs" hereafter. Slabs must be extended enough in the vertical direction to be optically thick to the N V, C IV resonance transitions yet must be dense enough as well for the upper and lower levels to attain departure coefficients not far from unity. We expect this density still to be 10^{10}–10^{11} cm^{-3} even though a proper model has not been constructed yet to describe the C IV line formation in the atmosphere of an early B star.

In setting up a dimple model-construct, we can make two other inferences. The first (Statement 1) is that dimples form well above the photosphere. The second (Statement 2) is that the ratio of the slab to stellar disk areas is equal to or larger than the ratio of dimple "absorption" to overall line strength. Statement 1 comes from the dimple-disturbance showing itself only in lines formed at the top of the atmosphere, viz. λ6678 and the C IV, N V lines. In contrast, other photospheric C, Si, and He II lines show no equivalent width changes. Thus, the dimple-causing instability shows a stratified response limited to the upper atmosphere. Statement 2 holds if the excitation temperature of λ6678 is zero. If $T_{\rm rad}$ is finite then the projected area of the dimple-disturbance will be even larger. If the slab in projection resembles a circle, then a 3% dimple absorption corresponds to a slab radius of $\leq 1\ R_\odot$. Given a time scale for the initial development of 15 minutes, the propagation velocity for the density instability is 800 km s^{-1}, or slightly higher if, as is likely, the line core is not black. This value is comparable to the lateral propagation velocity inferred from the appearance/disappearance of micro emissions in this profile at certain epochs (Smith 1991). Note this estimate is wholly empirical and does not depend on any physical mechanism. That the value is so much higher than the sound speed implies the existence of an external, spatially coherent "trigger" that causes the "condensation" of the slab, e.g., an Alfvén wave with a large damping length.

4.2. *The Scattering Mechanism*

The considerations stated above suggest that dimples are formed by scattering within a slab which is optically thick in

the λ6678 line (but not the continuum) and placed well above the stellar surface. Because the observations suggest that the line's equivalent width is constant to within errors, we consider simple scattering models in which all photons entering the slab are removed from the vertical line of sight. If we take a typical slab density, $\sim 10^{11}$ cm^{-3} (or even somewhat lower) from the UV line response, then complete redistribution across the line profile for a subordinate transition is all but assured. With these simplifications the problem reduces to a geometrical scattering with complete redistribution across the local intensity profile followed by a Doppler mapping of λ6678 radiation onto the rotating stellar disk.

Side and top views of the scattering geometry are shown in Figure 11. Photons emerging from the star first encounter the slab and are scattered isotropically off its lower edge. Even those photons initially scattered in forward directions will be virtually all rescattered backwards and eventually emerge from the slab's lower boundary. Of interest is the great majority of photons ultimately scattered at a low angle from the horizon toward a surrounding "penumbral" region. The column length is long in these directions so that by hypothesis the photons will eventually be scattered again either by a low-density "coma" surrounding the slab or by the penumbra's upper atmosphere owing to the shallow angle they make entering it. Those photons directly backscattered are absorbed and rethermalized by the photosphere directly beneath the slab. Evidently, most photons must be rescattered and escape the star or else or conservation of equivalent width would be violated (we justify this assumption by geometric modeling, as described below). Of course, from our vantage point as stationary observers the penumbral regions display different components of Doppler motion from the slab's due to the star's rotation. Thus, in our reference frame photons scattered are absorbed preferentially by one wing of the line and redistributed throughout the profile by the local Voigt profile. In the integrated profile we observe both photons emerging directly from the subpenumbra (photosphere) and those that are scattered in the penumbra, both at the same Doppler shift.

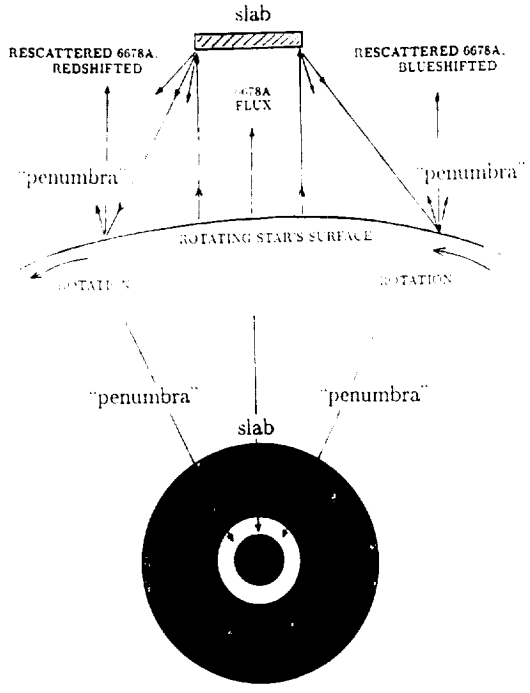

FIG. 11.—Schematic of dimple formation from backscattering of λ6678 radiation from an opaque (in the λ6678 line) "slab" suspended well over λ Eri. Upper panel represents view from the side; lower panel represents view from above the "slab" looking down. Backscattered line radiation illuminates a "penumbra" at shallow angles and is rescattered into the line of sight of the external observer. In the observer's frame these twice-scattered photons acquire the local projected rotational Doppler shift of the underlying star.

The result of these processes is that the line formed for lines of sight passing through the slab is nearly black whereas the lines of sight passing through the penumbra show incipient emission. The line flux for slab lines of sight must be different from the line flux (~45%) for the rest of the star. In fact it is the contrast between profiles formed from the slab-penumbral complex and the immaculate disk that produce the dimple's "absorption" component.

The processes just described can be conveniently represented in a Doppler integration computer code as follows. Denoting the bandwidth over which the line is optically thick as $\Delta\lambda_{dop}$, the emergent intensity from the slab is zero. If the slab is centered at the external observer's substellar point, the intensity is zero within the rectilinear limits $\pm x_{sl}$, $\pm y_{sl}$ given by the projected slab boundaries (generally circular, and for wavelengths in the range $\pm\lambda$ ($\lambda = 0$ at line center):

$$\mathcal{I}(\lambda, x, y) = 0 , \tag{1}$$

The net intensity gain at the bottom of the slab is likewise zero within these same x, y, λ limits. In our Doppler-mapping computations we will neglect the flux input from the penumbra, just as we will neglect the thermalization losses from photons backscattered to the occulted photosphere. Typically, these two terms tend to cancel, as we will justify below. The gain term, representing the upward flux of photons from the occulted photosphere, can be approximated by

$$\text{Flux to Slab} = \int_{-\Delta\lambda+\delta\lambda_{sl}}^{\Delta\lambda+\delta\lambda_{sl}} \int_{-y_{sl}}^{y_{sl}} \int_{-x_{sl}}^{x_{sl}} \mathcal{I}(\lambda, x, y) dx\, dy\, d\lambda , \tag{2}$$

where $\mathcal{I}(\lambda, x, y)$ is the local intensity profile of the occulted photosphere beneath the slab, and:

$$\Delta\lambda = 3.5\Delta\lambda_{Dop} ,$$

where $\delta\lambda_{sl} = V_{sl}\lambda_0/c$, the projected velocity of the slab relative to the penumbral regions.

By hypothesis these gains are balanced by photon scatterings from the slab (again temporarily ignoring true losses from thermalizations). There are given by

$$\text{Scattered Flux} = 2\int_{-y_{occ}}^{y_{occ}} \int_{-x_{occ}}^{x_{occ}} \int_{-\Delta\lambda+\delta\lambda_r}^{+\Delta\lambda+\delta\lambda_r} \frac{d\Omega_{pen}(x, y)}{d\Omega_{pen} + d\Omega_{occ}} \times \left[\frac{\mathcal{I}(\lambda, x, y)}{\mathcal{I}_c(x, y)}\right] \delta\mathcal{I}(\lambda, x, y) d\lambda\, dx\, dy , \tag{3}$$

where $d\Omega_{pen}$, $d\Omega_{occ}$ are projected penumbral and occulted-photosphere areal elements, respectively, as seen by an observer in the slab and where $\delta\lambda_r$ is the local projected Doppler shift from rotation. The ratio $[\mathcal{I}(\lambda, x, y)/\mathcal{I}_c(x, y)]$ is determined from the intensity line profile shifted by the projected rotational velocity in the penumbra toward the external observer. Upon equating equation (2) with equation (3), one can solve for $\delta\mathcal{I}(\lambda, x, y)$ at each point on the disk. These intensities can be combined with the nominal photospheric line profile

intensities across the disk to obtain a rotationally broadened profile with a simulated dimple.

The procedure just described contains a few obvious simplifications. The first is the complete redistribution assumed for scattering, which, as mentioned, is likely to be a good assumption for the densities contemplated. In our simulations we experimented with coherent scattering and have obtained nearly identical results to complete redistribution. This is true because the intrinsic intensity profile is nearly rectangular.

A second simplification is the issue of the loss of photons to the observer's line of sight, which can be tested by comparing the photon-in/photon-out budget to the slab from the entire photosphere. We wrote a computer program, ALLPATHS, to integrate all single-scattered photon paths from the star to the slab in order to assess the errors incurred by the oversimplified geometrical integration limits in equations (2) and (3). This program included effects of spherical curvature of the star and limb darkening. We allowed for one simplification, namely that all photons scattered in the directions between the local horizon and the local perpendicular to the vertical (a subhorizon zone) are rescattered isotropically by a low-density coma surrounding the slab. We believe this is a more realistic assumption than to postulate a slab with sharp edges, particularly in light of the response of the C IV, N V lines to a larger area over the star. The existence of a slab-coma could well explain why the λ6678 shows no change in equivalent width when dimples appear (cf. Table 1). In our formulation photon net gains to the penumbra due to the slab occur primarily because photons scattered off the slab to the subhorizon-zone are added in the gain/loss budget (isotropic scattering by an overlying coma) to those directed toward the penumbra. A small additional gain occurs because the photons initially emergent from the penumbral photosphere suffer modest limb-darkening losses that are not compensated by oppositely directed radiation (photons scattered a second time in the penumbra). The ALLPATHS results for several cases of interest are summarized in the form of a loss/gain budget in Table 3. The entries, suitably normalized to reflect the full 2π steradian integration limits for the slab-scattered flux, give the line flux from the penumbra to the slab (col. [2]), the scattered flux from all incoming light to the slab in the direction of penumbra and subhorizon (col. [3]), the emergent flux from the occulted photosphere plus the thermalization losses there after scattering from the slab (col. [4]), and the net percentage loss to the equivalent width of the line due to the presence of the slab (col. [5]: the sum of the first three columns). Not surprisingly, this table shows that the fractional losses of line radiation are largest for large slabs at low elevations. For typical parameters derived in § 4.4, namely: area = 3%, elevation = 10% of a stellar radius, the losses are on the order of 10%, and thus they fall within equivalent width measurement errors. At the same time these numerical experiments suggest that the elevations of the slabs probably are not less than $0.05R_*$. With this stipulation we are satisfied that the results of these experiments are consistent with the equivalent width conservation noted in Table 1. For this reason we used the simple geometrical scattering limits of equations (2) and (3) in our Doppler-remapping computations formulated in DIMPLE.

Because the backscattering mechanism operates only when the slab is optically thick to line photons, the scattering mechanism shuts off abruptly for slabs moving upward or downward at velocities larger than the line width, $\sim$45 km s^{-1}. This shutoff occurs because the slab scatters line-wing or continuum photons originating in the photosphere. These photons are transparent to photospheric scattering so when they reenter the photosphere under the penumbra they thermalize instead of scattering a second time. As a consequence, only a high-velocity absorption component remains in the profile. High-velocity absorptions are only rarely seen in this line, incidentally, and only when the star undergoes large-scale ejections such as discussed by Smith et al. (1991). The avoidance of dimples with high-velocity ejections is again consistent with the requirement of our mechanism that dimples represent a low radial velocity or stationary phenomenon. Hence, they cannot be associated, for example, with wind inhomogeneities.

4.3. *Model Atmosphere Considerations*

The reduced line flux emerging from slab lines of sight can come about in one of two ways: a low gas temperature in the slab, or a reduced ratio of departure coefficients of the atomic levels of λ6678. At this point we cannot eliminate either possibility, and as noted above do not believe we can constrain the slab temperature yet. Tests with Hubeny's TLUSTY code for a spherically-symmetric (slab-free) model atmosphere appropriate to λ Eri (24,000 K, log g = 3.9) show that the level populations for λ6678 begin to depart substantially from their LTE values just about where the line core is formed. Thus, $b_2/b_3 \sim 0.6$ at τ_c(Ross) $\sim 10^{-3}$, and $N_{gas} \sim 4 \times 10^{12}$ cm^{-3}). The b-ratio of the λ6678 transition barely changes up through the atmosphere (0.45, at $N \sim 10^9$ cm^{-3}) after its initial departure from unity. However, this is only true if the temperature in the upper atmosphere is not influenced by some yet unknown agent, be it line blanketing or magnetic fields! Regardless of the value of the departure coefficients, radiative deexcitations do prevail in the He I for superficial atmospheric layers. In essence, this means that any plasma having $N_{gas} < 4 \times 10^{12}$ cm^{-3} does indeed rescatter incident λ6678 photons.

To see whether our slab back-scattering picture is self-

TABLE 3

FLUX GAINS/LOSSES TO SLAB

Model Slab Area/Slab Elevation (1)	Flux from Penumbra (2)	Flux Return to Penumbra (3)	Thermal and Occultation Losses to Occulted Photosphere (4)	Fractional Equivalent Width Loss (5)
0.01/0.05.....	−0.633	0.940	−0.433	−0.126
0.03/0.05.....	−0.362	0.493	−0.496	−0.365
0.01/0.1	−0.681	0.793	−0.203	−0.091
0.03/0.1	−0.426	0.588	−0.293	−0.131
0.01/0.2	−0.592	0.648	−0.063	−0.007
0.03/0.2	−0.401	0.534	−0.120	−0.013

consistent, we have experimented further with ad hoc slabs using TLUSTY. Our models show that over a wide range of temperatures the λ6678 line forms in a slab when the total column density exceeds 8×10^{11} 2^1P-atoms cm^{-2}. If the slab thickness is assumed to be comparable to its slab diameter (2 $R_\odot$), and the excitation-ionization fraction is 5×10^{-10} (models), then the density required for an optical thickness of 10 in the line must be $\sim 2 \times 10^{11}$ cm^{-3}. This density estimate is sensitive to the slab optical depth, and in fact τ(slab) goes as N_e^2. It is encouraging that 2×10^{11} cm^{-3} is within an order of magnitude of the density inferred for the plasma responsible for the C IV, N V line weakening. Since the 10%–20% weakening is several times larger than the dimple strength (1%–4%), it is plausible that the "slab" is not a homogenous structure with well-defined edges, but rather that it consists of a dense nucleus in which λ6678 scattering occurs surrounded by a lower density periphery where the C IV line forms, as we argued above. Our models suggest that radiative losses from higher densities such as would be found in the slab can reduce the temperature by 2000–3000 K. Thus, for example, if one takes $\sim$12,000 K, for the slab's kinetic temperature, the line would have a line depth of 12%. The elevation of the slab above the star by $0.1R_*$ reduces the mean flux the slab sees, and this decreases the populations of the upper atomic levels further. Ironically, the overpopulation of lower He I states in our very hot slab models ($\sim$50,000 K) also shows slightly lower core depths than the nominal value (40%–45%), but more importantly it leads to excess line flux even well off (>0.5 Å) the line center. For either the hot- or cool-slab cases the effect of these non-LTE departures on the λ6678 line flux is substantial and appears to be far closer to 0% than to the nominal line flux of 40%–45% emerging from the photosphere outside the slab.

Having an understanding that the slab must be dense and opaque to λ6678 radiation, let us return to the Doppler mapping of the scattered line radiation.

4.4. *Doppler Mapping Results*

The geometrical-scattering and doppler mapping mechanism for the slab model was coded into a FORTRAN program DIMPLE. Specifically, this program computes an integrated flux profile using intrinsic profiles calculated at 20 center-to-limb positions and sums the line intensities across a two-dimensional model disk for each of 399 wavelengths. In our simulations we experimented with grids ranging from 50^2 to 200^2 elements in a square rectilinear coordinate system. DIMPLE also incorporates rotational broadening and instrumental blurring. For most applications we found that the grid spacing was not important for $\geq 100^2$ elements. The final ones presented are at the highest resolution. The intrinsic profile was taken from a $T_{\rm eff} = 25{,}000$, log $g = 4.0$ model with a microturbulence of 4 km s^{-1}. A damping constant was chosen that forced a match both with TLUSTY's computed profiles and the Heasley, Wolff, & Timothy (1982) profile of a slowly rotating B2 star, χ Cen. Photon scattering was simulated by computing a re-emissivity function at each grid point under the slab and in the surrounding "penumbra." This function is zero (infinite optical depth in the slab) within the slab area and exceeds unity in the penumbra by an amount proportional to the projected penumbral grid element. Doppler shifts were computed for each of the penumbral grid points according to the projected local velocity component of the line of sight to the external observer.

Within this construct models were computed with three free parameters. The first is the projected slab area, and the second the elevation of slab over the star. The area sets the strength of the absorption component, and is roughly equal to the deformation of this feature divided by the overall equivalent width. The second parameter sets the stellar limb (horizon) as seen from the slab and therefore the wavelength range of incipient emission over the dimple. The third parameter is the Gaussian velocity broadening assumed for gas in the slab. This parameter controls the shape of the dimple, giving it its almost cuspy appearance. (As noted above, if the slab plasma is hot, the intrinsic line profile may be broader and if so this parameter may actually be superfluous.) Figure 12 shows the effects of the primary (first two) parameters for a model with an exaggerated area and three widely varying values of slab elevation above the stellar surface.

Initially, we considered circular slabs at the center of a stellar disk. Our implicit assumption that the external observer is in the equatorial plane is probably a good assumption for λ Eri (Smith et al. 1991). These simple assumptions permitted the re-emissivity function to be computed in one dimension and axisymmetrized about the center. The geometry was later modified to include inclined slabs (which simulate reflections of "mirror-slabs"), slabs offset along the equator, and ellipsoidal slabs and penumbra. We will now describe the numerical experiments and give a few examples.

Figures 1 ("textbook"), 13, and 14 show three fits to observed dimples. Large-scale profile deformations outside the dimple, generally taken to come from nonradial pulsations, were not fitted in order to minimize the number of free parameters. By comparing trial models individually for the left and right halves of the dimple, we estimate internal errors in the slab areas and elevations to be $\pm$30% and (+100%, −50%). Once again, the range in elevation implied in our fits agrees with the observation that the equivalent width of the λ6678 line is conserved when dimples appear. Our models show, not surprisingly, that the absorption area under the immaculate profile approximately scales with the slab area. In models where the elevation of the slab is decreased to nearly zero, the scattered line flux is concentrated into narrow, bright emission spikes. Such spikes are never observed to accompany actual

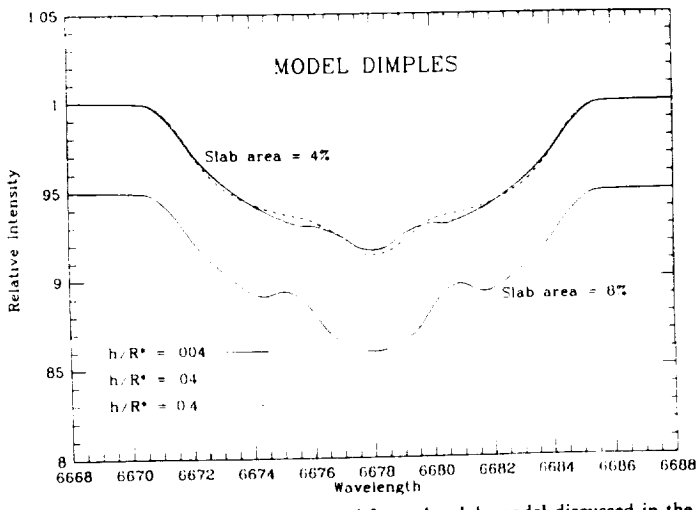

FIG. 12.—Model dimples computed from the slab model discussed in the text (see illustration in Fig. 11) for three values of the elevation h in stellar radii. The bottom frame shows the $h/R^* = 0.04$ model for an exaggerated slab area of 8% of the stellar disk.

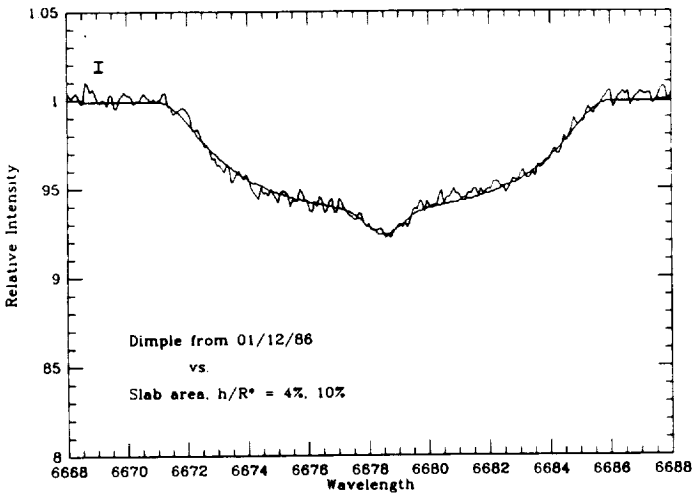

FIG. 13.—Fit to another well-defined dimple observed on 1986 January 12 at 5:19 UT with a Reticon.

dimples and their absence helps constrain the estimated elevations of slabs above the star. As the elevation decreases at first the fraction of photons returned to and thermalized in the occulted photosphere is small. However, as also implied by Table 3, as the elevation decreases further the fraction of photons thermalized becomes large so that the emission weakens. Eventually only an absorption feature remains, and the line strength increments by essentially the slab/disk area. The different appearance of the profile resulting from a change in slab elevation suggests that the "*type d*" (narrow stationary absorption) features we reported in S89 are caused by a similar phenomenon as dimples, namely by opaque slabs but at very low elevations. The slightly shorter lifetime (1–2 hr) of *type d* features is consistent with this interpretation.

Our initial set of models assumed that the intrinsic intensity profiles of material in the slab have the same square shape as photospheric profiles. Figure 15 shows that such models produce absorption features that are flat-bottomed, unlike the observations. Next we experimented with ellipsoidal slabs with the long axis oriented in the polar direction of the stellar disk.

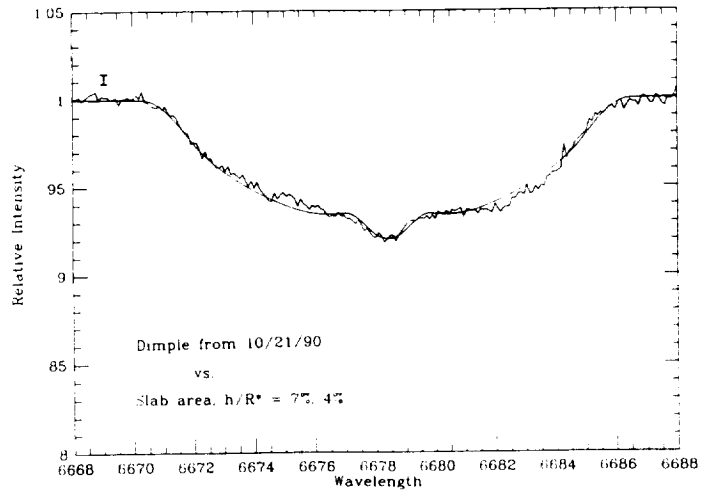

FIG. 14.—Fit to a yet another observed dimple observed on 1990 October 21 at 11:35 UT. The poor fits outside the dimple are due to profile distortions from nonradial pulsation.

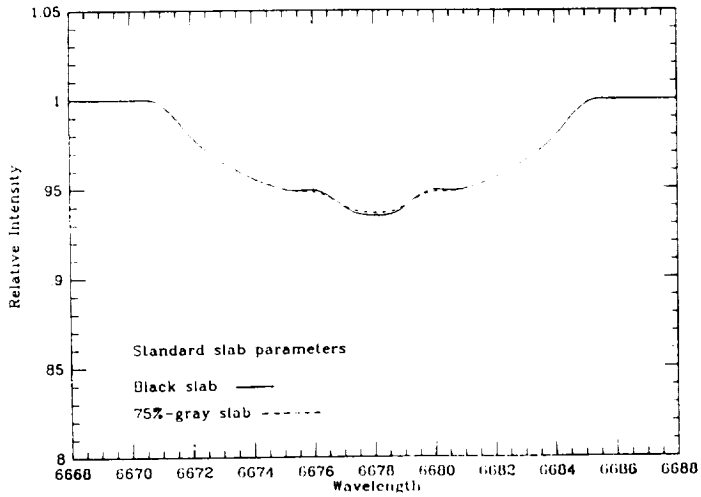

FIG. 15.—Comparison of slab models that are completely opaque (photospheric intrinsic profile assumed, for illustration of broad core) and translucent. The translucent profile (*dashed line*) "leaks" 25% of upward λ6678 photons at the slab center and all of them at the edges.

Ellipsoidal slabs do lead to more cuspy absorption features but only if the major/minor axis ratio is extreme. Thus, we were able to get reasonable fits to cuspy-absorptions, of which Figure 13 is a good example, but *only* if the ratio of ellipsoidal axes is 30:1. It was this contrived geometry that led us to abandon long narrow shapes and adopt instead an internal Gaussian broadening as the third parameter in our slab models. The cuspy absorptions can be fit only by Gaussian parameters of 2–2.5 Doppler widths. This parameter was used in all the fits shown herein.

A key question as to the origin of dimples is the mass of a typical "slab." We cannot determine this from λ6678 profiles alone because the slab is already assumed to be infinitely optically thick. We have tried to contrive ways of estimating whether the optical thickness is closer to unity than infinity by looking for edge effects in slab models. Figure 15 shows a model in which only 75% of photons are backscattered from the center of the slab and zero at the edges. Except for a slight increase in line strength, the effect is to diminish the contrast between the absorption and emission features. As this is similar to the effect of decreasing the slab area, we found that there is a trade-off between slab area and photon leakage. A second aspect of a nonopaque slab is that the border between the slab and penumbra can be expected to be gradational. Thus, as an additional test we simulated gray-border effects by permitting the emissivity function to decrease quadratically from one to zero from the center to edges of the slab. The results are very similar to standard models run with slightly smaller slab area. Models with a more diffuse (linear) transition produced dimples with a decreased absorption/emission contrast, as in Figure 15.

Occasionally, dimples exhibit very unequal blue/red emissions. In extreme cases the stronger emission on one side of the dimple can show an inversion while the other emission is much weaker. We have investigated a variety of models that might reproduce inverse P Cygni-like features such as we observed on 1987 February 6 (see below). We were successful in simulating this peculiarity with two constructs. The first assumed a slab tilted 45° to the horizontal that scatters line photons preferentially toward the receding or approaching limb of the star

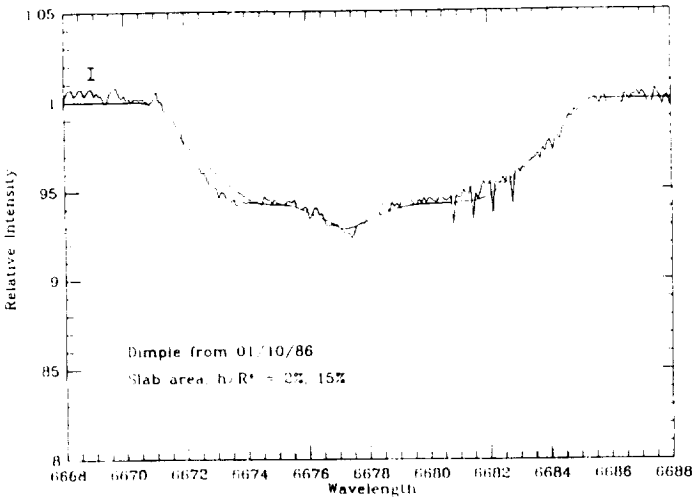

FIG. 16.—Fit to a slab off-set from the stellar disk center. This profile is indistinguishable from a model with a disk-centered slab rising at $+15$ km s^{-1}.

like a "mirror." One side of the penumbra then experiences an illumination by backscattered radiation while the other side is occulted by the slab. Our experiments suggest that this contrivance can work, but only nonlinearly. We were able to reproduce approximate matches to Figure 16 but only if the elevations of the lower and upper edges of the mirror showed ratios of about 20. We consider this such slab orientations to be farfetched, and we dropped this geometry from our consideration.

A more natural way to reproduce P Cygni-type features is to permit the slab to fall or rise at some velocity. If the slab corotates over the star, the problem is not edifying because one cannot distinguish between a falling/rising slab at disk-center and a stationary slab located off-center and toward a stellar limb. To make the case more interesting, we allowed the model slab to move laterally over the star contrary to the sense of rotation (i.e., the slab is fixed along the line connecting the observer to the center of the star). The horizontal velocity creates a vectorial addition problem because the slab velocity now shares two orthogonal motions with respect to each stellar areal element. As is always true with Doppler mapping, the vectorial addition breaks the spatial symmetry of isokinetic contours on the stellar disk, so that a dimple with asymmetric emissions forms. For small velocities (≤ 20 km s^{-1}) the effects are unremarkable in our models. Thus, Figure 16 shows that slowly rising/falling slabs mimic models of stationary slabs located slightly off disk center. In this case both the emissions and the absorption are symmetrical around the projected local velocity. (A falling slab moving parallel to the polar axis would produce the same dimple.) As already discussed, for velocities greater than the line width (45 km s^{-1}) the backscattered photons are lost and only an absorption feature remains. The interesting regime is for velocities just less (absolute value) than the line width. The steep gradient of the line then makes itself felt most strongly. A falling slab experiences a blueshift from photospheric radiation and therefore sees increased flux in the blue wing ("line-center flux" to the slab observer). A correspondingly greater line flux is backscattered and reemitted into the external observer's line of sight from elements on the stellar disk with the same projected velocity. In this case the number of illuminated elements on the "red" side of the disk is reduced. The net result is that the aggregate reemitted line flux is still conserved in these models, except that it is now redistributed preferentially onto a spatially asymmetric isokinetic contour of the penumbra. As the velocity approaches the intrinsic line width this area becomes centrally concentrated in a small zone at the same stellar latitude as the slab. This confined area accounts for the sharp emissions of these "P Cygni" dimples.

Figure 17 shows a falling-slab model fit to two consecutive observations of an "inverse P-Cygni" dimple in the λ6678 profile. Note that between the midpoints of the two observations, 1.3 hr, there is no evidence that the dimple has evolved substantially. In this time the slab would have fallen $0.04R_*$, so there is no real contradiction to our solution for the mean height $0.1R_*$. In fact the velocity we derived and this time interval suggest together that our elevation is probably a lower limit. Otherwise, the good fits to this peculiar shape by the addition of a "natural" parameter confirms the basic premise that dimples arise from Doppler mapping of rescattered line radiation. However, we must add a caveat to this optimistic conclusion that a second, lateral velocity in the direction of rotation is required to explain the asymmetric dimples. We do not propose to address in this paper the question of what could propel the slabs at the implied horizontal velocities (~ 80 km s^{-1}). Indeed, this may provide an important hint of their formation mechanism. For the present we will point out that if the slabs's horizontal velocities are random then there must be many slabs that are moving in the "north-south" direction, and if so their horizontal velocities cannot be observed. Thus we cannot rule out that the majority of the slabs are slowly returning to (or rising from) the surface of λ Eri.

5. CONCLUSIONS: WHAT DIMPLES MAY AND MAY NOT REPRESENT

We have examined a simple model in which backscattered λ6678 radiation is Doppler shifted by rotation across the stellar disk. The scattering process allows photons initially removed by a thick slab to reemerge from a surrounding "penumbral" region surrounding the slab. The result is that weak emissions to the blue and red sides of an absorption feature are formed in the λ6678 profile, and a "dimple" is born.

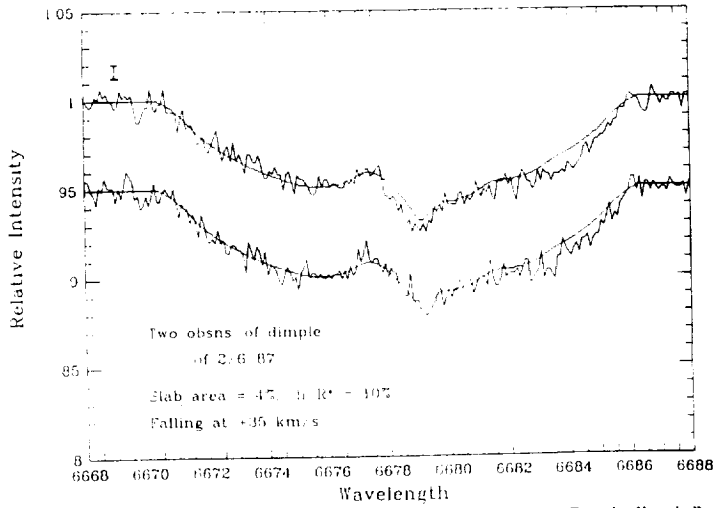

FIG. 17.—Consecutive observations of an "inverse P Cygni dimple" matched with a slab model falling at 35 km s^{-1}. Because these two observations were made with a now obsolete Reticon detector, each of them required a 75 minute integration time.

We have exhibited representative examples of fitted models to dimples and have shown that only three parameters are necessary to fit three attributes of dimples, namely a slab area (accounting for the dimple absorption strength), the slab elevation over the star (the extent of the incipient emission in wavelength), and the doppler motions of the gas in the slab (absorption component's shape and width).

We do not claim that the basic backscattering/Doppler mapping mechanism is unique. Still, we are encouraged that so simple a formulation can provide such good matches to the observations at this level of approximation. Aside from the fits to the profiles themselves, three observations tend to support our picture:

1. Stars listed in Table 2 as showing dimples in their λ6678 lines are all rapid rotators. This implies that Doppler mapping from rotation is an essential component of the dimple mechanism.

2. The ability of the model to mimic (inverse/) P Cygni profile dimples with falling/rising slabs provides a valuable independent test of its predictive capacity.

3. The existence of pure absorption (*type d*) profile transients can be understood naturally by this concept as an extension to cases where slabs are close to the star. Then most of the scattered photons will be lost through thermalization in the photosphere directly beneath the slab, and the dimple becomes a true absorption.

It is reasonable to conjecture that slabs come into being as a result of explosive events located beneath the star's surface. Although ad hoc, this line of thought is instructive because one can at least predict the consequences of ballistic ejections. However, at least three arguments can be made against ballistic ejecta being responsible for dimples in λ Eri. First, dimples last too long for the slabs to be moving under gravity alone. For the parameters we adopt for λ Eri ($10\ M_\odot$, $6\ R_\odot$), the total time elapsed for a *ballistic* ejection corresponding to a maximum height of $\sim 0.1 R_*$ is only 2.0 hr. The time during which an ejection would spend at less than 45 km s^{-1} is only 0.39 hrs. Even for a maximum height of $0.2R_*$ the time is still only 0.47 hr. These times are far shorter than the lifetimes of dimples, and therefore they argue against ballistic motions. Second, a ballistic ejection would show dimple signatures caused first by a rising (P Cyg emission profile), stationary (symmetric emission), and finally a falling (inverse P Cyg) projectile/slab. However, none of our observations of dimples have ever shown this sequence; dimples do not evolve that way. Third, the example shown in Figure 17 indicates a falling slab with no apparent acceleration over 1.3 hr. A ballistic infall would show obvious acceleration over this time. Instead, there seems to be a buoyant or levitating force that prevents the slab from accelerating.

A related alternative is that slabs are orbiting circumstellar debris (or "spokes") transiting the disk. Actually this is merely a variant of our basic model, differing phenomenologically only in that the "lifetime" of the slab is set by the transit time across the disk. However, there are several difficulties with this picture. The first problem is that dimples are observed to change shape as they first develop, as noted above, whereas an orbiting blob would merely manifest itself as a transiting feature on the profile. (The "P Cygni" dimples in particular could not be explained in this manner.) Second, the transit time scale must then be close to 8 hr, rather longer than dimples are observed to last. Third, slabs must have long lifetimes according to this scenario, perhaps on the order of days. Condensed structures could not be expected to last much longer than an orbital time scale given the numerous forces (tidal, viscuous, thermal, and radiation pressures, magnetic stresses?). Fourth, the sudden appearance of multiple dimples at different places on the profile is particularly difficult to explain by orbiting blobs. Fifth, and finally, the *reduced* frequency of dimples during λ Eri's mass-loss phases would be difficult to explain in this picture.

The above considerations rule out rather firmly that dimples can be the results of mass tossings, explosive events on the surface, or orbiting debris. One alternative is that they arise from a series of rapid mini-ejections, all lasting a few hours. We cannot rule out this idea. A second possibility is that dimples manifest instabilities in which plasma "condenses" from ambient low-density plasma and remains suspended over the star. Indeed, this is the current explanation of quiescent prominences in the solar corona. The prominence condensations arise from the plasma thermal instability, which is reponsible for plasma existing in either a hot (10^6 K) or cool (10^4 K) state. Prominences are thought to be suspended above magnetic arches which act as a buoyant cushion. Without speculating fürther about magnetic processes on Be stars, we point out that the elevation of the slabs and their high densities relative to ambient plasma are similar to values obtained for solar prominences. In addition, dimple structures seem to grow some 40 times as fast as ionization or recombination waves propagate (speed of sound). Yet, Alfvén velocities may attain as high a value as the magnetic field warrants. For a density $N_{gas} \sim 2 \times 10^{11}$ cm^{-3} and an Alfvén velocity of 800 km s^{-1}, a value of $B \sim 160$ G is implied.

Finally, minimum masses of slab structures can be estimated by assuming a minimal optical depth of one, a slab radius of 1 $R_\odot$, and a column density of 2.5×10^{-3} gm cm^{-2}, as computed by TLUSTY. The resulting mass is $\sim 2 \times 10^{-14}\ M_\odot$. Non-LTE models of the Hα line constructed by M. Marlborough for a $0.2R_*$ slab suspended over a star with parameters appropriate to λ Eri also suggest masses of about $10^{-14}\ M_\odot$. Such models would produce emission of only ~ 35 mÅ, or about 4 times weaker than the detection threshold for emission in our data. Therefore, they may not be observable as Hα emission. At any given time, there are likely to be on average at least $1\frac{1}{2}$ slab structures distributed anywhere over surface of λ Eri. Thus the minimum mass tied up in slab structures in an "exo-photosphere" of λ Eri is likely to be $\sim 3 \times 10^{-14}\ M_\odot$. Even though this estimate relies on a generously lower limit for the slab's optical depth, it already constitutes more mass than is present above depths of $\tau_c \sim 6 \times 10^{-6}$ of the star's atmosphere.

Future searches for dimples in weaker He I lines will settle whether, as we suspect, our mass estimate is too low by a factor of 10 or more. However, even allowing for liberal errors in this estimate, there is clearly a problem in explaining how so much material can be brought out to the exo-photosphere. Once again, this is similar to the enigma of solar prominences: there are too many condensing dense structures for this matter to come from the total ambient coronal plasma. The solution for λ Eri, as for the Sun, may lie in matter rising continuously over the entire "quiescent" disk. Perhaps this matter is responsible for the "second penumbral scattering" in our basic dimple model. Even if such flows were visible in He I lines, they would be difficult to observe directly in broad Be profiles. However, they could cause conceivably small line asymmetry signatures that could be inferred relative to motions of common proper

motion companions or through an ensemble radial velocity determined for many mild Be stars.

Further efforts will be undertaken by MAS, T Meylan, I. Hubeny, and T. Lanz to compute more self-consistent models of slab conditions. Additionally, the typical slab size, density, and disturbance propagation velocity derived herein together suggest that a time delay of several minutes might occur between the appearance of a dimple in λ6678 and in weaker subordinate transitions. We plan to exploit these stratification effects by monitoring the concomitant development of dimples in λ6678 and subordinate lines in the 2^1P series.

We wish to express our gratitude to I. Hubeny for permitting us to use his program TLUSTY and quote results. It is our pleasure to acknowledge particularly helpful conversations on the "slab mechanism" with D. Baade, A. Fullerton, K. Gayley, I. Hubeny, and T. Meylan as well as seminal discussions with S. Shore. We also greatly appreciate M. Marlborough's computing non-LTE models of Hα emission of model slabs. We are indebted in an anonymous referee for advising us on clearer presentations in the figures and also for correcting a misunderstanding we had on the scattering off high-velocity slabs. We thank J. Holberg for help in the preparation and reduction of *Voyager* data. We also acknowledge a number of allocations of McMath telescope time from the National Solar Observatory's TAC and some dedicated rapid-cadence coverage of this line by Paul Avellar. This work was carried out in part under the auspices of NASA grants NAS5-28749 and NAS5-31221.

REFERENCES

Anderson, L. S. 1985, ApJ, 298, 848
Bjorkman, J. E., & Cassinelli, J. P. 1992, in Nonisotropic and Variable Flows from Stars, ed. L. Drissen (Dordrecht: Kluwer), 88
Heasley, J. N., Wolff, S. W., & Timothy, J. G. 1982, ApJ, 262, 663
Hubeny, I. 1988, Comput. Phys. Comm., 52, 103
Lamers, H. J., & Pauldrach, A. W. 1991, A&A, 244, L5
Longo, R., Stalio, R., Polidan, R. S., & Rossi, L. 1989, ApJ, 339, 474
Pauldrach, A. W. 1987, A&A, 183, 295
Pauldrach, A. W., Puls, J., Kudritzki, R. P. 1986, A&A, 164, 86
Peters, G. J. 1991, in ESO Conf. Proc. 36, Rapid Variability in B Stars: Nature and Diagnostic Value, ed. D. Baade (Garching: ESO) 171
Polidan, R. S., & Holberg, J. B. 1987, MNRAS, 225, 131
Sakhibullin, N. A., & van der Hucht, K. 1983, Soviet Astron., 27, 529
Smith, M. A. 1989, ApJS, 71, 357 (S89)
———. 1991, in ESO Conf. Proc. 36, Rapid Variability in OB Stars: Nature and Diagnostic Value ed. D. Baade (Garching: ESO), 59
Smith, M. A., Peters, G. J., & Grady, C. A. 1991, ApJ, 367, 302
Waters, Ł. B., & Marlborough, J. M. 1992, A&A, 263, 195
Waters, L. B., van der Veen, W. E., Marlborough, J. M., & Dougherty, S. M. 1991, A&A, 244, 120

REPORT DOCUMENTATION PAGE

Form Approved
OMB No. 0704-0188

1. AGENCY USE ONLY *(Leave blank)*	2. REPORT DATE	3. REPORT TYPE AND DATES COVERED
	March 1995	Contractor Report

4. TITLE AND SUBTITLE

Voyager GO Program

5. FUNDING NUMBERS

Code 684.1
S ~~97228-E~~ 97229-E
Task 5797

6. AUTHOR(S)

Principal Investigator: Myron Smith

7. PERFORMING ORGANIZATION NAME(S) AND ADDRESS(ES)

Computer Sciences Corporation
4061 Powder Mill Road
Calverton, MD 20705

8. PERFORMING ORGANIZATION REPORT NUMBER

RHPU0428

9. SPONSORING/MONITORING AGENCY NAME(S) AND ADDRESS(ES)

NASA Aeronautics and Space Administration
Washington, D.C. 20546-0001

10. SPONSORING/MONITORING AGENCY REPORT NUMBER

CR-189435

11. SUPPLEMENTARY NOTES

Technical Monitor: D. West, Code 684.1

12a. DISTRIBUTION/AVAILABILITY STATEMENT

Unclassified-Unlimited
Subject Category: 89
Report available from the NASA Center for AeroSpace Information,
800 Elkridge Landing Road, Linthicum Heights, MD 21090; (301) 621-0390.

12b. DISTRIBUTION CODE

13. ABSTRACT *(Maximum 200 words)*

This contract pertained to the investigation of the time variability of the ultraviolet continuum flux of three stars, lambda Eri, 53 Persei, and gamma Cas. The observation were conducted in 1991 and were provided to the Principal Investigator in December 1992. The investigator travelled to Tucson, Arizona to reduce to the data in February of 1993 and analyzed the data during the spring and summer of 1993.

14. SUBJECT TERMS

lambda Eri, 53 Persei, gamma Cas, Voyager GO

15. NUMBER OF PAGES

2 (plus appendicies)

16. PRICE CODE

17. SECURITY CLASSIFICATION OF REPORT	18. SECURITY CLASSIFICATION OF THIS PAGE	19. SECURITY CLASSIFICATION OF ABSTRACT	20. LIMITATION OF ABSTRACT
Unclassified	Unclassified	Unclassified	Unlimited

Publications from Contract:

Smith, M. A., and Polidan, R. S. 1993, "Dynamic Processes Be Star Atmospheres II. "Dimple Formation in the HeI 6678A Line of lambda Eri," ApJ, 408, 323.

Smith, M. A., and Huang, L. 1994a, "NRP Mode Typing for 53 Persei: Results from Voyager Photometry," Rotation, Pulsation, and Mass Loss, ed. L. Balona and H. Henrichs, (Dordrecht: Kluwer), p. 37.

Smith, M. A. 1994b, "Photospheric Activity in Selected Be Stars," Rotation, Pulsation, and Mass Loss, op. cit., p. 241.

Smith, M. A., 1995, "Dynamic Processes Be Star Atmospheres III. Rapid Multi-Wavelength Variability in Gamma Cas," ApJ, 492, --- (4/1/95).